

# Surface Reactions and Catalytic Activities for Small Alcohols over $\text{LaMnO}_3(100)$ and $\text{La}_{0.7}\text{Sr}_{0.3}\text{MnO}_3(100)$ : Dehydrogenation, Dehydration, Oxidation

*Yafen Zhang, David R. Mullins,\* Aditya Savara\**

Chemical Science Division, Oak Ridge National Laboratory, Oak Ridge, Tennessee 37831-6201, United States

**Notice:** This manuscript has been authored by UT-Battelle, LLC, under contract DE-AC05-00OR22725 with the US Department of Energy (DOE). The US government retains and the publisher, by accepting the article for publication, acknowledges that the US government retains a nonexclusive, paid-up, irrevocable, worldwide license to publish or reproduce the published form of this manuscript, or allow others to do so, for US government purposes. DOE will provide public access to these results of federally sponsored research in accordance with the DOE Public Access Plan (<http://energy.gov/downloads/doe-public-access-plan>)..

## ABSTRACT

The surface chemistry and catalytic activity of small alcohols (methanol, ethanol, propan-2-ol) were studied over  $\text{LaMnO}_3(100)$  and  $\text{La}_{0.7}\text{Sr}_{0.3}\text{MnO}_3(100)$  thin films. The observed C-containing products corresponded to products typically associated with dehydrogenation (methanal, ethanal, propanone), dehydration (ethene, propene), and oxidation ( $\text{CO}_x$ ). No coupling products were observed. Two types of temperature programmed reaction experiments (TPR) were performed: Pre-exposure TPR (PE-TPR) experiments in which the reactant is pre-adsorbed and the temperature is then ramped, as well as continuous exposure TPR (CE-TPR) experiments during which the reactants are continuously introduced and the temperature is ramped. Mechanistic pathways are proposed based on the results and literature, including removal of lattice oxygens by surface hydrogens, organic intermediates adsorbed in oxygen vacancies, C-H bond breaking by alkoxy disproportionation reactions, and direct C-H bond breaking. The vacancy related pathways are suppressed by the Sr substitution. The data are interpreted to indicate that Sr substitution causes vacancies to bind adsorbates less strongly, resulting in decreased catalytic activity for the vacancy mediated reactions in the study. Sr substitution increases the ratio of alkene production to aldehyde/ketone production. Catalytic turnover frequencies are reported for the C-containing products for the temperatures of 650 and 750 K for both surfaces.

## 1. Introduction

ABO<sub>3</sub> perovskite-type mixed oxide catalysts are increasingly studied due to their great flexibility with respect to tailoring their redox properties and their efficiency in the oxidation of hydrocarbons<sup>1-3</sup> and other species<sup>3-6</sup>. In some cases, perovskites have been suggested as an alternative to metal catalysts.<sup>7</sup> The role of the A-site's rare-earth ions (Ln) in the reducibility and the behavior of the oxygen in the perovskite's structure has been studied by Misono and co-workers in the context of oxidation of propane and methanol.<sup>8</sup> They found that the trivalent rare-earth elements had no effect while the B-site metal played a primary role in controlling the catalytic activity for oxidation.<sup>9</sup> However, the partial substitution of A cations by lower valence cations could result in the generation of structural defects, such as anionic (O-vacancies) or cationic vacancies.<sup>1, 10-11</sup> For example, a partial substitution of La by Sr would be expected to decrease the energy of formation corresponding to B cation vacancies or oxygen vacancies to the perovskite structure, thereby facilitating oxygen transport and reducibility.<sup>8, 12-14</sup> The surface chemistry in the presence of such substitutions, and the role of the O-vacancies in surface chemistry is not yet well studied.

The chemical reactions of interest include partial oxidation of alcohols to produce aldehydes, ketones, or acids (for chemicals production). Complete oxidation of organic oxygenates is also of interest for vehicular and other air pollution control. There are publications in the literature suggesting that the adsorption and reaction of simple alcohols on metal oxide catalysts can be used as fundamental chemical probe reactions.<sup>15-19</sup> For example, it has been suggested that methanol undergoes dehydration to form dimethyl ether on acidic surface sites and dehydrogenation on redox/basic sites to produce methanal or CO<sub>2</sub>.<sup>19</sup> However, detailed

studies of chemistry on reducible oxides provide greater chemical complexity than this simple picture would suggest, when vacancies are present.<sup>14, 18, 20-36</sup>

In this work, two compositions of perovskite thin films,  $\text{LaMnO}_3(100)$  and  $\text{La}_{0.7}\text{Sr}_{0.3}\text{MnO}_3(100)$  are studied for reactions with methanol, ethanol, and propan-2-ol. Two different types of temperature programmed reaction measurements were conducted, during which the gas phase is monitored for reactant and product molecules. In *pre-exposure* temperature programmed reaction (PE-TPR), often referred to as temperature programmed desorption, less than one monolayer of reactant is adsorbed and then the sample temperature is ramped while monitoring the gas phase species evolved. This type of experiment evaluates the strength of interaction between the alcohol and the surface, the stability of surface-bound intermediates, and the reaction products of those intermediates. In *continuous exposure* temperature programmed reaction experiments (CE-TPR) the surface is continually exposed to reactant gas while the sample temperature is increased. The study includes continuous exposure experiments with  $\text{O}_2$  in the feed as well without  $\text{O}_2$  in the feed. The CE-TPR experiments enable observing pathways and catalytic activity that occur via short-lived surface species at elevated temperatures, which are not necessarily observable in PE-TPR. The CE-TPR experiments also enable constant chemical potential across the experiments for varying ratios of reactants (in this case, the alcohol :  $\text{O}_2$  ratio). The objective of this study is to explore how the reactivity and selectivity of these alcohols varies after 30% substitution of La with Sr, and also to provide insights about the chemical mechanisms that transpire on these perovskite surfaces.

## 2. Experimental and Characterization

A model  $\text{LaMnO}_3(100)$  ( $\text{LaMnO}_3(100)$ ) catalyst was prepared as a thin film grown on 0.05% Nb-doped  $\text{SrTiO}_3(100)$  ( $\text{STO}(100)$ ) by pulsed laser deposition (PLD).<sup>14</sup> The film was

grown using an  $\text{LaMnO}_3$  target with a laser fluence of  $\sim 1.5 \text{ J cm}^{-2}$  while the substrate was heated up to  $650 \text{ }^\circ\text{C}$  in a background pressure of 200 mTorr  $\text{O}_2$ . The film growth was monitored by reflection high-energy electron diffraction (RHEED) that indicated an  $\text{LaMnO}_3$  film thickness of  $\sim 20 \text{ nm}$ . The single-crystalline nature of the  $\text{LaMnO}_3(100)$  film was determined by thin film X-ray diffraction (XRD) and the film thickness was confirmed by the thickness fringes in the high-resolution  $\theta - 2\theta$  scans of the (002) diffraction peaks (“Epitaxy” software, Panalytical). An  $\text{La}_{0.7}\text{Sr}_{0.3}\text{MnO}_3(100)$  thin film of was grown to a thickness of  $\sim 20 \text{ nm}$  on a 0.05% Nb-doped  $\text{STO}(100)$  by PLD using the same conditions, as reported previously.<sup>14, 37</sup> Thus, both films were  $\sim 20 \text{ nm}$  in thickness. Atomic force microscopy and RHEED images are available in reference<sup>14</sup>.

Excitation energy dependent XPS was conducted on Beamline 23-ID-2 (CSX-2) at NSLS II. The La 4d ( $\sim 100 \text{ eV}$ ), Sr 3d ( $\sim 130 \text{ eV}$ ) and Mn 3s ( $\sim 80 \text{ eV}$ ) were monitored at different photon energies. The core levels have similar binding energies and therefore similar escape depths at the photon energies utilized. The ratios of the integrated intensities were determined and normalized to the ratio measured at the highest photon energy where the ratio presumably reflects the composition of the cations in the bulk. These ratios are shown in Fig. 1.

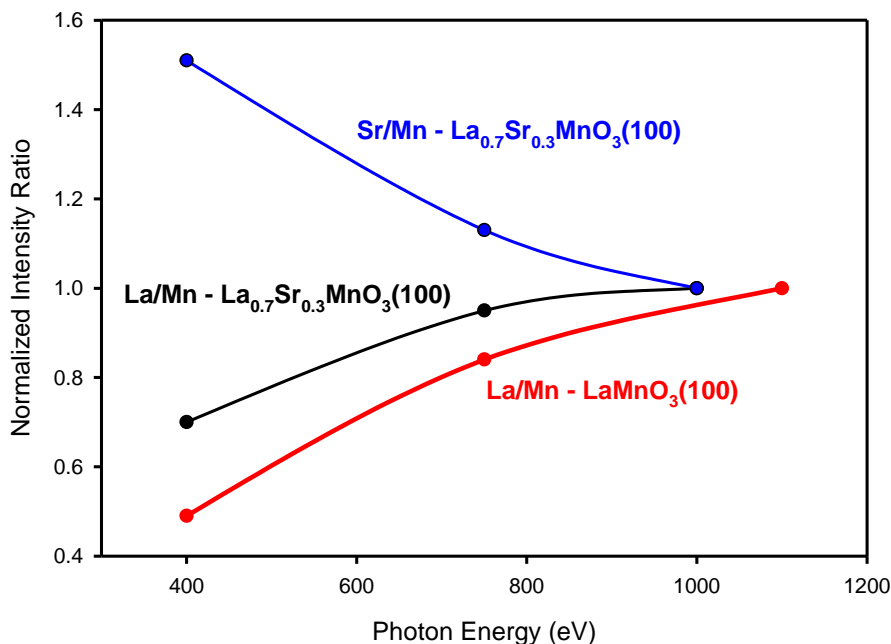


**Figure 1.** Excitation energy dependent XPS of the Sr 3d, La 4d, and Mn 3s photoemission peaks indicate that the surface of  $\text{LaMnO}_3(100)$  and  $\text{La}_{0.7}\text{Sr}_{0.3}\text{MnO}_3(100)$  surfaces are each enriched in Mn relative to La, and that the surface of  $\text{La}_{0.7}\text{Sr}_{0.3}\text{MnO}_3(100)$  is enriched in Sr.

For  $\text{LaMnO}_3(100)$  the ratio of La to Mn decreases at smaller photon energy indicating that the La concentration is lower than the Mn concentration at the surface than it is in the bulk. For  $\text{La}_{0.7}\text{Sr}_{0.3}\text{MnO}_3(100)$  the Sr to Mn ratio is greater at smaller photon energies indicating that Sr is enriched at the surface relative to the composition in the bulk. The La to Mn ratio is smaller at the surface compared to the bulk but the difference is not as great as in  $\text{LaMnO}_3(100)$ . This is likely due to the decreased Mn concentration at the surface. We are not aware of a systematic study for such thin films grown by pulsed layer deposition, these enrichments may not be true of all thin films prepared by the same method and with the same nominal composition. For the two samples being studied, it would be expected that the samples have an Mn layer termination (rather than La layer termination)<sup>38-39</sup>. The observation that the sample with Sr substitution has

some level of enrichment within the layers near the surface (relative to the bulk), is consistent with prior<sup>40-43</sup> publications. There can, in general, be changes in the stability of the terminating layer/phase as a function of the oxidation potential.<sup>44-47</sup> There may also be some form of strontium oxide particles (“islands”) on the surface,<sup>40-43</sup> though Sr islands blocking a portion of the surface would not be sufficient to explain the qualitative differences observed below.

Prior to temperature programmed reaction experiments, the model surfaces were first cleaned by oxidation in  $\sim 10^{-6}$  Torr of O<sub>2</sub> at 800 K for at least 30 min. XPS measurements at the synchrotron indicated that this treatment was sufficient to remove C from the surface. The oxidized surface was then exposed to  $\sim 7$  L of alcohol from an effusive doser<sup>48</sup> at 190 K. This temperature was chosen to be slightly higher than the typical multilayer desorption temperatures of the alcohols.<sup>49</sup> During temperature-programmed reaction experiments, the gas phase molecules were monitored using a Hiden HAL/3F 301 mass spectrometer at Oak Ridge National Lab (ORNL). The PE-TPR experiments occurred in a “line-of-sight” normal direction<sup>50</sup> geometry with the sample face  $\sim 2$  cm away from the mass spectrometer aperture and the temperature was ramped at 2 K/s. During these experiments, the sample was biased -70 V to prevent electrons generated by the mass spectrometer ionizer from stimulating reactions at the surface.<sup>27, 51-52</sup> For CE-TPR experiments, alcohol and O<sub>2</sub> were mixed in a stainless steel ballast with the ratio of alcohol:O<sub>2</sub> as either 1:0 or 1:1 before directly dosing onto the surface through the effusive gas doser. The 1:1 ratio thus refers to backing pressure but can be considered as nominal 1:1 ratio regarding the effective pressures experienced by the surface. Based on gas uptake measurements at low temperature, and on the rate of pressure decrease in the ballast, the effective pressure on the samples were on the order of  $\sim 10^{-6}$  torr. The fluxes on the samples are dependent on reactant mass and are calculated to be  $8.73 \times 10^{18}$  molecules m<sup>-2</sup> s<sup>-1</sup>,  $7.27 \times 10^{18}$

molecules  $\text{m}^{-2} \text{s}^{-1}$ , and  $6.39 \times 10^{18}$  molecules  $\text{m}^{-2} \text{s}^{-1}$  for methanol, ethanol, and 2-propanol, respectively. Knowledge of the flux of reactants and products along with the number of surface sites enables turnover frequencies to be calculated.<sup>53</sup> During CE-TPR, the temperature was ramped at  $1 \text{ K/s}$  from an initial temperature of  $300 \text{ K}$ .

Reactants and products were monitored with the following representative masses:  $\text{H}_2$  ( $m/z = 2$ ),  $\text{H}_2\text{O}$  ( $m/z = 18$ ),  $\text{CH}_2=\text{CH}_2$  ( $m/z = 27$ ),  $\text{CO}$  and others ( $m/z = 28$ ),  $\text{CH}_3\text{CHO}$  ( $m/z = 29$ ),  $\text{CH}_2\text{O}$  ( $m/z = 30$ ),  $\text{CH}_3\text{OH}/\text{CH}_3\text{CH}_2\text{OH}$  ( $m/z = 31$ ),  $\text{CH}_3\text{CH}=\text{CH}_2$  ( $m/z = 41$ ),  $\text{CO}_2$  ( $m/z = 44$ ),  $\text{CH}_3\text{CH}(\text{OH})\text{CH}_3$  ( $m/z = 45$ ),  $\text{CH}_3\text{C}(\text{O})\text{CH}_3$  ( $m/z = 43$  and  $58$ ). The data were smoothed prior to analysis. Overlapping fragments, such as methanol and methanal at Mass 30 or ethene and  $\text{CO}$  at Mass 28, were corrected by subtracting a known proportion of a unique mass from the overlapping mass. For example, 1.6 times the value of the signal at Mass 27 was subtracted from the signal at Mass 28 to remove the ethene contribution at Mass 28. The resulting intensities were converted to relative concentrations by multiplying the corresponding PE-TPR traces by scale factors according to the method proposed by Ko and Madix.<sup>54</sup> Though this method enables converting mass spectrometry signals to relative concentrations, there is some error: based on our experience, on the order of 30% error is not unusual, and thus perfect mass balance is not expected. Improving the scaling method is one direction of research in our group.

### 3. Results and Discussion

#### 3.1. Reactions of Methanol on $\text{LaMnO}_3(100)$ versus $\text{La}_{0.7}\text{Sr}_{0.3}\text{MnO}_3(100)$

Methanol is a commonly used alcohol for studying catalysis over metal oxides with the intent of gaining fundamental information about the chemistry and the nature of the active sites.<sup>18-19, 55</sup> The temperatures at which products are observed in PE-TPR provide information

that can be used to assess the most likely rate-limiting steps during chemical conversions.<sup>24</sup> Here, we initially employ methanol as a probe molecule to explore the catalytic activity of the two perovskite single-crystal surfaces, then move to ethanol and propan-2-ol.

### 3.1.1. PE-TPR of Methanol

Fig. 2 shows the PE-TPR results following methanol adsorption at 190 K on  $\text{LaMnO}_3(100)$  and  $\text{La}_{0.7}\text{Sr}_{0.3}\text{MnO}_3(100)$ .

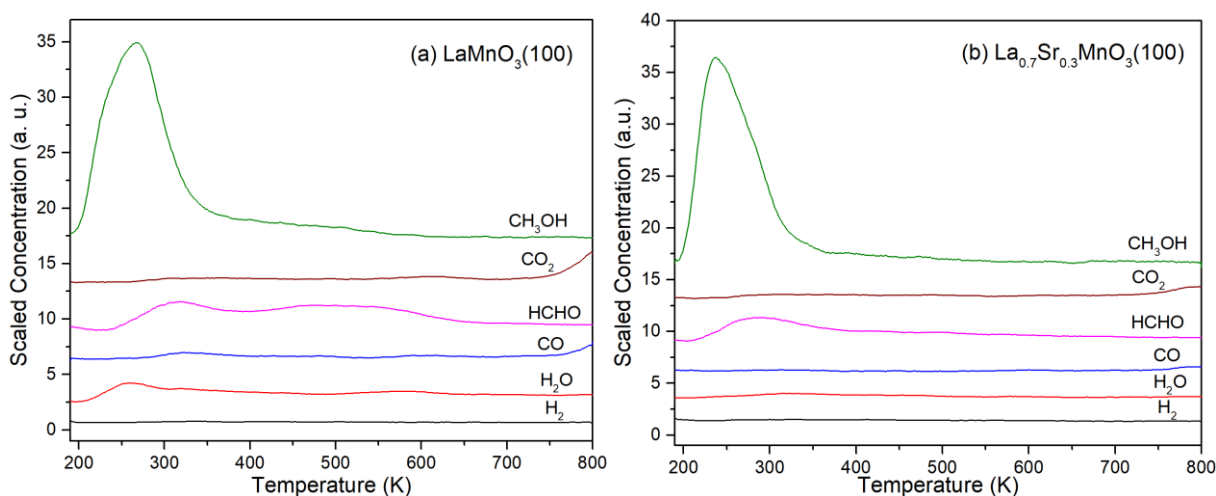
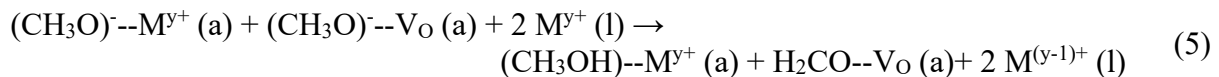
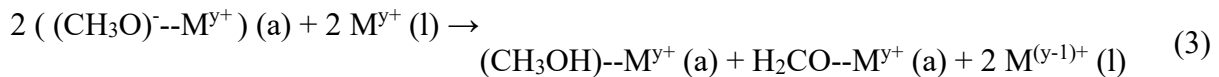
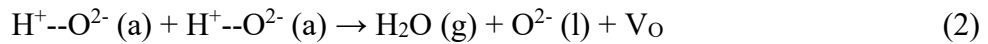
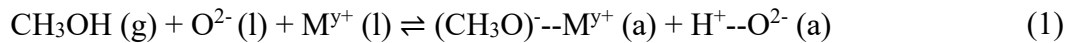


**Figure 2.** PE-TPR spectra following the adsorption of methanol at 190 K on pre-oxidized (a)  $\text{LaMnO}_3(100)$  and (b)  $\text{La}_{0.7}\text{Sr}_{0.3}\text{MnO}_3(100)$ .

Based on the temperature range, the methanol desorption peak at  $\sim 270$  K from  $\text{LaMnO}_3(100)$  in Fig 1a is likely due to desorption of molecularly adsorbed methanol and/or from recombination of adsorbed methoxy and surface hydrogen (Eq. 1).<sup>20, 22, 24, 38, 56-57</sup> One of the reviewers pointed out that if this alcohol is produced via a recombination reaction, the peaks for gas phase alcohol should shift to higher temperatures with lower initial coverages, in accordance with expectations for a TPR with a second order reaction between surface species.<sup>58</sup> While we

did not systematically study the effects of coverage dependence, we did obtain some data to ensure that the pre-exposures being used were adequate: those data are shown in the supporting information and do show the expected trend for a recombination reaction (that lower coverages result in a higher peak maximum temperature). The presence of methoxy from dissociation of methanol is also supported by the observation that water is produced below 300 K which results from the reaction of surface hydrogens with lattice oxygen (Eq. 2):<sup>35, 56, 59-60</sup> such surface hydrogens are generated from dissociative methanol adsorption.<sup>20-21, 23, 38, 57</sup> As a result, the consumption of surface hydrogens creates O vacancies, which may further stabilize methoxy groups present on the surface.<sup>21, 61-62</sup> The methoxy groups present undergo further reactions at higher temperatures including methoxy disproportionation to form methanal: based on theoretical results obtained over cerium oxide, the mechanism is likely via Eq. 3) at ~300 K and likely via Eq. 5) at ~500 K.<sup>21</sup> The mechanism proposed for methanal production is a redox mechanism, consistent with prior characterization of methanol reactions on oxides.<sup>19</sup> For Eq. 5), the reaction is written as producing an aldehyde in an O-vacancy, as the methanol attributed to Eq. 5) is observed at a slightly lower temperature than the aldehyde, and this interpretation is consistent with calculations on cerium oxide.<sup>21</sup> The  $\geq$  ~500 K temperature range is also sufficient that there may a contribution from direct<sup>21, 34-35, 59, 61-64</sup> CH bond breaking from an alkoxy in an O-vacancy (Eq. 6).





In the above equations, species marked by (g) represent gas phase species, species marked by (l) represent lattice species, and species marked by (a) represent an adsorbed state in which the species on the left side of the double-dash is the adsorbate and the species on the right side of the double-dash is a lattice species or lattice vacancy.  $\text{V}_\text{O}$  represents an oxygen vacancy and  $\text{M}^{y+} (\text{l})$  represents a lattice cation. The ‘charges’ shown on the adsorbates and lattice species represent those associated with oxidation states and not true charges. In interpreting the oxidation states shown, it should be recognized that the oxidation state of O has a value of -2 in both  $(\text{CH}_3\text{O})^-$  and  $\text{CH}_3\text{OH}$ , and that this notation does not indicate any gain (or loss) of electron density for the oxygen. Similarly, the oxidation state of each hydrogen in  $\text{CH}_3\text{OH}$  and also in  $\text{H}^+$  is the same: the notation of  $\text{H}^+$  does not indicate any loss (or gain) of electron density. In the equations, additional surface cations are utilized for oxidation state charge balance and do not imply full charge transfer. How oxidation state notation is applied for adsorbates on oxide surfaces is further discussed in the supporting information. We note that the surface adsorbed hydrogens and also the surface alkoxy adsorbates are more likely<sup>20, 23, 38</sup> closer to net zero charge per adsorbate rather than unit charge, but still have partial charges.

Methanol recombination and reaction by the above pathways seems to occur on  $\text{La}_{0.7}\text{Sr}_{0.3}\text{MnO}_3(100)$  as well, as seen in Fig. 2b. There is less  $\text{H}_2\text{O}$  produced over the  $\text{La}_{0.7}\text{Sr}_{0.3}\text{MnO}_3(100)$  sample than over  $\text{LaMnO}_3(100)$  sample: as such, it seems that fewer O vacancies are created on  $\text{La}_{0.7}\text{Sr}_{0.3}\text{MnO}_3(100)$  to help stabilize the adsorbed methoxy. This may be the reason for less production of methanal at higher temperatures (500 – 600 K) on  $\text{La}_{0.7}\text{Sr}_{0.3}\text{MnO}_3(100)$  (Fig. 2b), relative to what is observed on  $\text{LaMnO}_3(100)$  (Fig. 2a). The

decreased H<sub>2</sub>O production (if occurring by Eq. 2) does not necessarily mean decreased thermodynamic reducibility as a result of Sr incorporation: a decrease of Eq. 2 may be due to a kinetic limitation,<sup>21, 35, 59</sup> regardless of whether the Sr increases the facility of reduction. The CO and CO<sub>2</sub> that are produced above 750 K may result from the oxidation of a small amount of dehydrogenated C species or carbonate type species.

### 3.1.2. CE-TPR of Methanol with and without O<sub>2</sub>

We investigated the reactivity during the continuous exposure of methanol on the two thin-film surfaces with and without O<sub>2</sub>. Temperature-programmed reaction (CE-TPR) experiments were performed while dosing the reactant gases onto the pre-cleaned LaMnO<sub>3</sub>(100) and La<sub>0.7</sub>Sr<sub>0.3</sub>MnO<sub>3</sub>(100) surfaces. During the experiments, the methanol flux was  $8.73 \times 10^{18}$  molecules m<sup>-2</sup> s<sup>-1</sup>, equal to a pressure of  $2.44 \times 10^{-6}$  Torr ( $3.25 \times 10^{-4}$  Pa) with respect to the number of molecules colliding with the surface per unit time. The O<sub>2</sub> concentration was set at either 0% or 100% of the methanol concentration. The green dotted lines in Fig. 3 indicate the response for a methanol “blank” to assess methanol consumption.

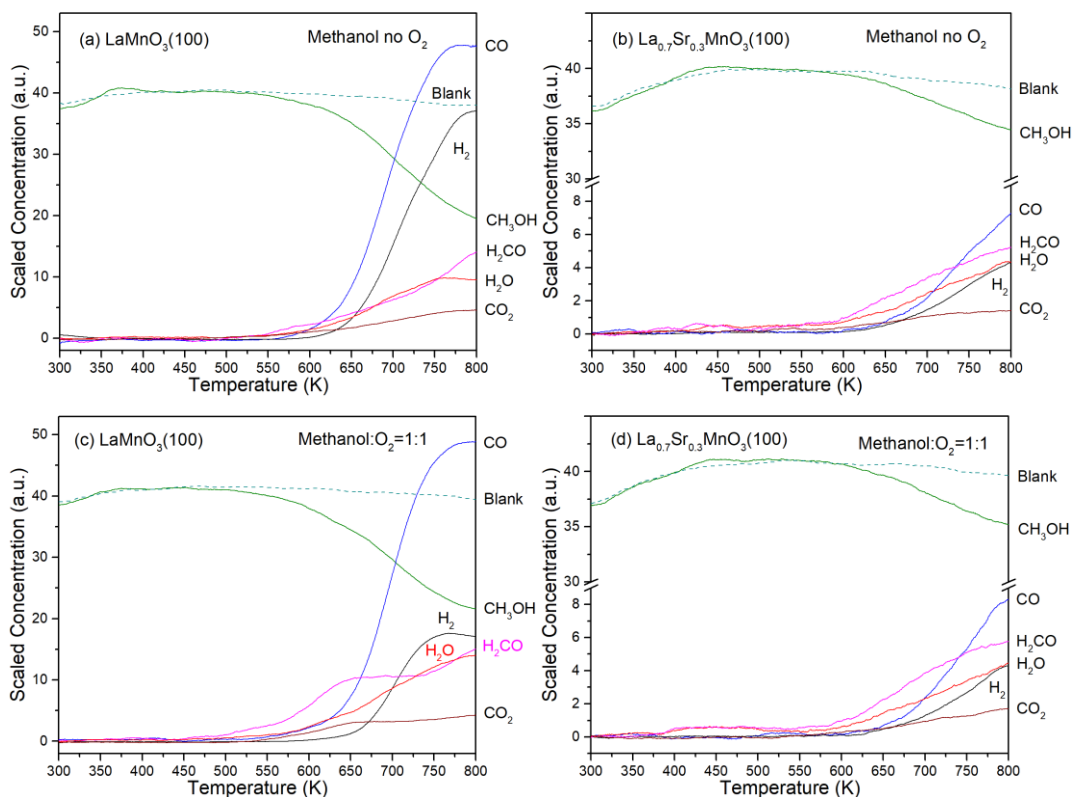


**Figure 3.** CE-TPR of methanol on  $\text{LaMnO}_3(100)$  and  $\text{La}_{0.7}\text{Sr}_{0.3}\text{MnO}_3(100)$  with the methanol: $\text{O}_2$  ratio set at 1:0 or 1:1. a)  $\text{LaMnO}_3(100)$  and Ratio of 1:0, b)  $\text{La}_{0.7}\text{Sr}_{0.3}\text{MnO}_3(100)$  and ratio of 1:0, c)  $\text{LaMnO}_3(100)$  and Ratio of 1:1, d)  $\text{La}_{0.7}\text{Sr}_{0.3}\text{MnO}_3(100)$  and ratio of 1:1.

As shown in Fig. 3a, in the absence of  $\text{O}_2$ , methanol on  $\text{LaMnO}_3(100)$  produced CO and  $\text{H}_2$  as the major products accompanied by smaller amounts of  $\text{H}_2\text{CO}$ ,  $\text{H}_2\text{O}$ , and  $\text{CO}_2$ . The onset of methanol depletion is at  $\sim 520$  K, which coincides with the production of methanal and water. Although the activity is low, the selectivity initially favors methanal. The water formation is likely with hydrogens produced when methanol dissociatively adsorbs on the surface. The water formation occurs with removal of lattice O: in the absence of oxygen, this pathway is not sustainable, and that may be the reason for the downturn of  $\text{H}_2\text{O}$  production above 750 K in Fig. 3a (the downturn in  $\text{H}_2\text{O}$  production does not occur in the presence of oxygen, in Fig. 3c). The

continued acceleration of H<sub>2</sub>CO production with temperature could be due to the surface reverting back to a redox character by O diffusion from the bulk to the surface, or could be due to direct CH bond breaking<sup>21, 34-35, 59, 61-64</sup> occurring at higher temperatures.

During the reaction of methanol on La<sub>0.7</sub>Sr<sub>0.3</sub>MnO<sub>3</sub>(100) (Fig. 3b), the onset of noticeable methanol depletion shifts to a higher temperature (~580 K) compared to the reaction of methanol on LaMnO<sub>3</sub>(100) -- and at all temperatures the products' intensities are significantly smaller than those during the reaction of methanol on LaMnO<sub>3</sub>(100) (note the change in scale in Fig. 3b compared to Fig. 3a). This indicates that the Sr substituted sample has less reactivity for methanol conversion under these conditions. The ratio of H<sub>2</sub>CO/CO is greater on La<sub>0.7</sub>Sr<sub>0.3</sub>MnO<sub>3</sub>(100) than on LaMnO<sub>3</sub>(100): while this can be interpreted as another sign of less reactivity, this observed selectivity towards less oxidized products may be a desirable trait for some applications. As on LaMnO<sub>3</sub>(100), the rate of CO and H<sub>2</sub> formation on La<sub>0.7</sub>Sr<sub>0.3</sub>MnO<sub>3</sub>(100) increases significantly with surface temperature.

In the presence of O<sub>2</sub>, the relative product ratios change. On LaMnO<sub>3</sub>(100), as shown in Fig. 3c, The production of H<sub>2</sub>CO starts at a lower temperature (~500 K), which could be attributed to the fact that O is filling in O-vacancies created by water desorption thus enabling the Eq. 3) to be sustained, which may have a lower activation energy than Eq. 5).<sup>21, 35</sup> The feature which resembles a local maximum at ~650 K in Fig. 3c was reproducible. At higher temperatures, above 730 K, the effect of oxygen on methanal production has largely disappeared, though H<sub>2</sub> production is suppressed. The data is consistent with the O<sub>2</sub> filling O-vacancies, which can have two consequences on the hydrogen production: a) decreasing O-vacancy assisted pathways to H<sub>2</sub> formation, and b) enabling some of the surface hydrogen intermediates to react with lattice oxygen when it is available to produce H<sub>2</sub>O. The changes in product distribution may

again be affected by the diffusion of oxygen from the bulk to the surface, with an increasing influence possible as the temperature approaches 800K. The influence of O<sub>2</sub> during the reactions of methanol on La<sub>0.7</sub>Sr<sub>0.3</sub>MnO<sub>3</sub>(100) is much less evident than on LaMnO<sub>3</sub>(100).

### **3.2. Reactions of Ethanol on LaMnO<sub>3</sub>(100) versus La<sub>0.7</sub>Sr<sub>0.3</sub>MnO<sub>3</sub>(100)**

The introduction of a C-C bond into the alcohol opens new possibilities for the reaction products during catalysis that are not present during the oxidation of methanol on the perovskite surfaces. For example, dehydration of ethanol will result in the formation of a C=C double which isn't possible for C1 methanol molecules. More complete oxidation to CO and CO<sub>2</sub> requires cleavage of the C-C bond in addition to the dehydrogenation of the C-H bonds. Investigations in complete oxidation of ethanol to CO<sub>2</sub> and H<sub>2</sub>O have attracted attention due to the demand for an efficient decontamination of exhaust pollutants produced by alcohol-fueled vehicles.<sup>65-66</sup> Further, the partial oxidation of ethanol has been studied to develop processes to produce ethanal or acetic acid.<sup>67-68</sup>

#### **3.2.1. PE-TPR of Ethanol**

PE-TPR spectra following ethanol adsorption at 190 K on oxidized LaMnO<sub>3</sub>(100) and La<sub>0.7</sub>Sr<sub>0.3</sub>MnO<sub>3</sub>(100) are shown in Fig. 4.

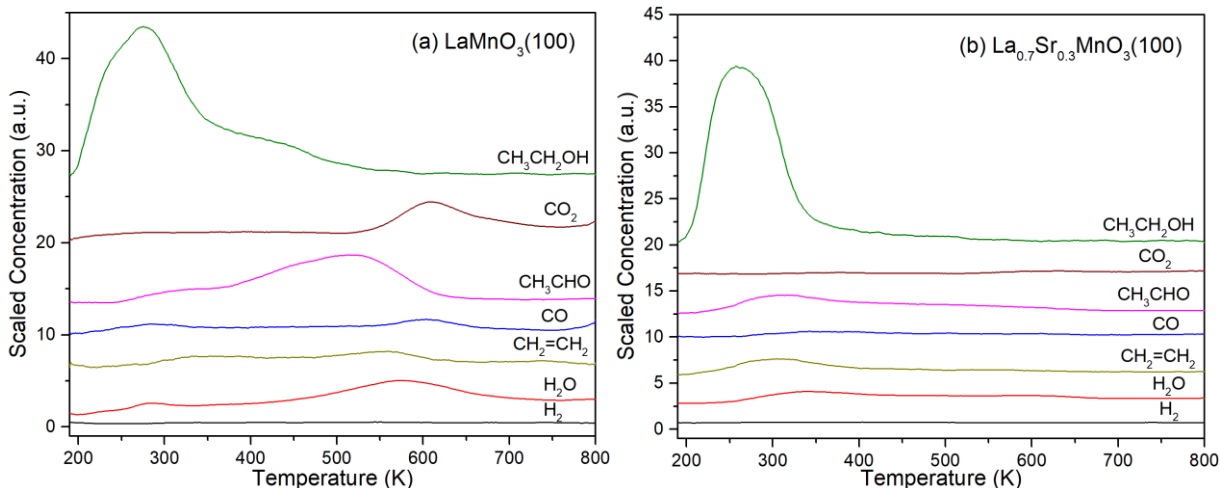
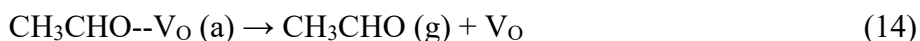
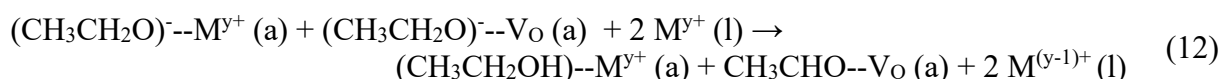
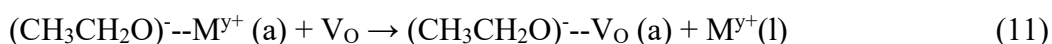
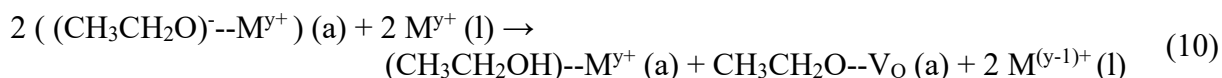
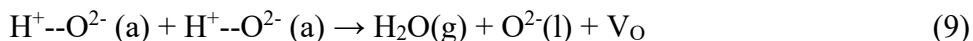
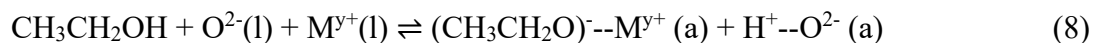


**Figure 4.** PE-TPR spectra following the adsorption of ethanol at 190 K on pre-oxidized (a)  $\text{LaMnO}_3(100)$  and (b)  $\text{La}_{0.7}\text{Sr}_{0.3}\text{MnO}_3(100)$ .

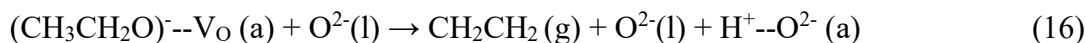
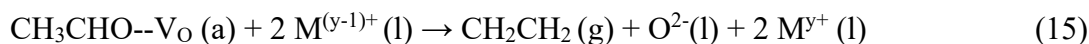
On  $\text{LaMnO}_3(100)$  (Fig. 4a) ethanol desorbs in a broad peak, with a low temperature feature centered around 275 K and a second feature extending to  $\sim 500$  K. The ethanol desorption observed is similar to what was observed with methanol, though the feature extending to 500K is more pronounced with ethanol. There are trace amounts of ethanal, ethene, and water desorbing below 400 K. A large fraction ( $> 10\%$ ) of the C-containing products is observed to be ethanal produced between 400 K and 600 K: this could be from Eq 9, 11 or 12. As was the case for methanol, there is an alcohol peak / shoulder observed at a slightly lower temperature than the aldehyde ( $\sim 425$  K versus  $\sim 500$ K). The temperature range where the aldehyde product is observed suggests that an aldehyde intermediate is bound in an O-vacancy, produced either from a disproportionation type reaction with an alkoxy oxygen as the hydrogen acceptor (Eq. 12) *or* from a direct C-H bond breaking that occurs with the lattice oxygen as the hydrogen acceptor (Eq. 13). Note that although ethanal is the dominant pathway, there is little  $\text{H}_2$  observed. This is presumably because the stoichiometrically produced H reacts with lattice O of the pre-oxidized

sample to produce water (along with O vacancies). At the same time, new water production is observed at ~575 K in quantities greater than was observed with methanol, and the new water is correlated with alkene production. The water is thus likely to be at least partially from stoichiometry equivalent to alcohol dehydration to alkene (such as Eq. 16 followed by Eq. 9). Given the significant ~500 K aldehyde production without concomitant H<sub>2</sub> production, the higher temperature H<sub>2</sub>O could also indicate that there is a pathway via a pair of reactions with stoichiometry equivalent<sup>21, 69</sup> to disproportionation, without being a true disproportionation. For example (as mentioned), we cannot exclude the possibility that the 500 K aldehyde comes from direct<sup>21, 34-35, 59, 61-64</sup> CH bond breaking from an alkoxy in an O-vacancy (Eq. 13). Similar to methanol, we arrive at the following set of chemical reaction equations (with reaction 2 reproduced as Eq. 9 for clarity). The notation is as described below Eq. 7.



Masses associated with the alkene (ethene) are produced in two ranges: 300-400K and 500-650 K. It is plausible for alkene formation to either go through or not go through an aldehyde intermediate. In either case, the proximity of the alkene and water peaks in Fig. 3a are consistent with some portion of the alkene production occurring from alkoxy and other

intermediates with conventional dehydration stoichiometry, likely via surface hydrogen intermediates (e.g., Eq. 16 followed by Eq. 9).



When the surface temperature rose above 600 K, oxidation of surface intermediates to combustion-like products occurred: CO, CO<sub>2</sub>, and H<sub>2</sub>O. These O-rich products stoichiometrically require reduction of LaMnO<sub>3</sub>(100) and could thus not be catalytically sustained without an oxygen source.

On La<sub>0.7</sub>Sr<sub>0.3</sub>MnO<sub>3</sub>(100) (Fig. 4b), the same reactions may be present, but the selectivity observed is more strongly biased towards < 400 K ethanol desorption (the same trend between surfaces as was observed for methanol). Given the differences observed, LaMnO<sub>3</sub>(100) appears to show more redox activity for these pathways relative to La<sub>0.7</sub>Sr<sub>0.3</sub>MnO<sub>3</sub>(100), with the former behaving more like CeO<sub>2</sub>(111) than the latter.<sup>24-25</sup>

### 3.2.2. CE-TPR of Ethanol with and without O<sub>2</sub>

The reactivity during the continuous exposure of ethanol on the two thin-film surfaces was investigated with and without O<sub>2</sub> by CE-TPR. The ethanol flux was equivalent to that of 7.27 x 10<sup>18</sup> molecules m<sup>-2</sup> s<sup>-1</sup>, equal to a pressure of 2.44 x 10<sup>-6</sup> Torr (3.25 x 10<sup>-4</sup> Pa) with respect to the number of molecules colliding with the surface per unit time. The O<sub>2</sub> concentration was set at either 0% or 100% of the ethanol concentration. The results are shown in Fig. 5, along with the ‘blank’ ethanol signal to assess ethanol consumption.

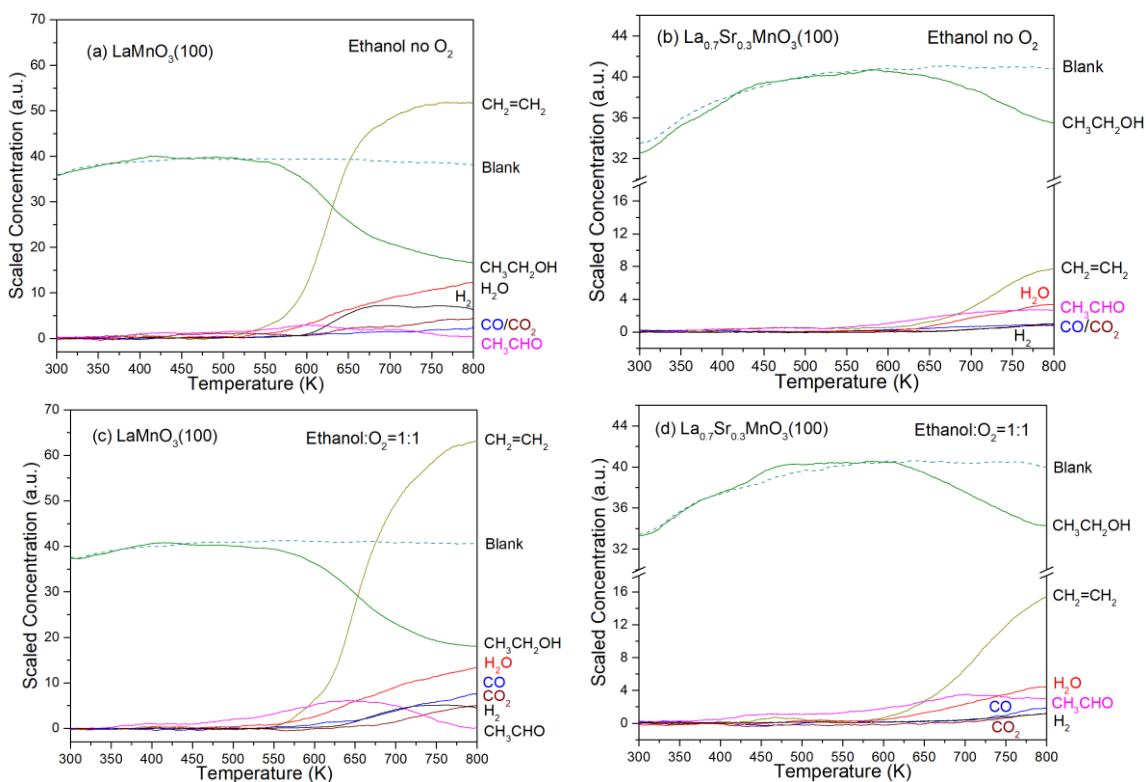


**Figure 5.** CE-TPR of ethanol on  $\text{LaMnO}_3(100)$  and  $\text{La}_{0.7}\text{Sr}_{0.3}\text{MnO}_3(100)$  with the ethanol: $\text{O}_2$  ratio set at 1:0 or 1:1. a)  $\text{LaMnO}_3(100)$  and Ratio of 1:0, b)  $\text{La}_{0.7}\text{Sr}_{0.3}\text{MnO}_3(100)$  and ratio of 1:0, c)  $\text{LaMnO}_3(100)$  and Ratio of 1:1, d)  $\text{La}_{0.7}\text{Sr}_{0.3}\text{MnO}_3(100)$  and ratio of 1:1.

On  $\text{LaMnO}_3(100)$  in the absence of co-fed  $\text{O}_2$  (Fig. 5a), dehydration of ethanol dominates and ethene is formed as the major product. This is perhaps surprising considering the observation that dehydrogenation to ethanal was the dominant reaction path observed in PE-TPR (Fig. 4a). This switch from dehydrogenation in PE-TPR to dehydration in CE-TPR is likely due to the reduction of the surface during the ethanol reaction and the concentration of surface species as the reduction occurs. Initially dehydrogenation may be the dominant pathway, but this is transient with reduction occurring rapidly resulting in ethene as the dominant product. The sustained production of  $\text{CH}_3\text{CHO}$  in greater quantities when oxygen is present in the range of

400-800 K (Fig. 5c) supports this interpretation. It is tempting, and overly simplistic, to conclude that the dominance of ethene indicates that the surface is acidic. Presumably less electron-deficient  $\text{Mn}^{3+}$  is less acidic than  $\text{Mn}^{4+}$ . However, the O vacancy makes the Mn under-coordinated. This stabilizes the ethoxy intermediate, hence the products appear at a higher temperature in CE-TPR compared to PE-TPR, and the surface competes with the adsorbate for the O. Also note that it is easier to dehydrate ethanol (to break the C-O bond and remove H, which produces a stable product, ethene) than it is to dehydrate methanol which requires coupling to produce a stable product.

On  $\text{La}_{0.7}\text{Sr}_{0.3}\text{MnO}_3(100)$  in the absence of oxygen (Fig. 5b), the onset of ethanol depletion is at  $\sim 600$  K which is about 100 K higher than that on  $\text{LaMnO}_3(100)$ , and the reactant consumption and total product intensities are considerably smaller, indicating less reactivity of ethanol on  $\text{La}_{0.7}\text{Sr}_{0.3}\text{MnO}_3(100)$  than on  $\text{LaMnO}_3(100)$  (note the change in scale). The ethene to ethanal ratio is lower on  $\text{La}_{0.7}\text{Sr}_{0.3}\text{MnO}_3(100)$  than on  $\text{LaMnO}_3(100)$  during CE-TPR (Fig. 5a versus Fig. 5b and Fig. 5c versus Fig. 5d). While it may be counterintuitive, this result is actually in line with the observation of greater ethanal production over  $\text{LaMnO}_3(100)$  during PE-TPR at  $\sim 500$  K (Fig. 4a vs Fig. 4d): the ethene in Fig. 5 and the  $\sim 500$  K aldehyde in Fig. 4 are each representative of products from intermediates in oxygen vacancies. The decrease in ethene formation in Fig. 5 is thus interpreted as being due to fewer intermediates in vacancies (likely due to fewer vacancies) during reaction conditions. The observation of more CO,  $\text{CO}_2$ , and  $\text{H}_2\text{O}$  over  $\text{LaMnO}_3(100)$  relative to  $\text{La}_{0.7}\text{Sr}_{0.3}\text{MnO}_3(100)$  additionally suggests greater steady state oxygen redox cycling for the  $\text{LaMnO}_3(100)$  sample. Other than these significant differences, the qualitative behavior observed is similar for the  $\text{LaMnO}_3(100)$  and  $\text{La}_{0.7}\text{Sr}_{0.3}\text{MnO}_3(100)$  samples.

In the presence of O<sub>2</sub>, the product selectivities change over LaMnO<sub>3</sub>(100). The presence of oxygen increases the CO<sub>x</sub> formation, aldehyde formation, and the > 700K alkene formation. The presence of oxygen suppresses the formation of H<sub>2</sub> relative to H<sub>2</sub>O (in contrast to what was observed for methanol). The suppression of H<sub>2</sub> formation may be due to the dehydration pathway that has opened to form the alkene, such that less hydrogen reaches the surface. Effectively, ethene production (with water as a co-product) may deplete the intermediates which would otherwise lose hydrogen in abstraction steps to make H<sub>2</sub>. In both the absence and the presence of O<sub>2</sub>, the H<sub>2</sub> and aldehyde productions go through maxima. The maxima of the aldehyde production are likely due to competition with the alkene pathway, suggesting that the alkene pathway has a higher activation energy (which is consistent with the PE-TPR experiments). Although the alkene is likely produced from intermediates in O-vacancies, the presence of gaseous oxygen increases alkene production: presumably this is due to having increased activity with the right ‘balance’ of O-vacancies to surface lattice oxygens, as the surface lattice oxygens can perform hydrogen abstraction (such as in Eq. 16). The decrease of H<sub>2</sub> production as the temperature is raised even further is presumably due to the temperature becoming high enough that surface H are able to directly extract lattice oxygens, similar to what has been observed over cerium oxide.<sup>70</sup> Over La<sub>0.7</sub>Sr<sub>0.3</sub>MnO<sub>3</sub>(100) the presence of oxygen similarly increases the CO<sub>x</sub> formation, aldehyde formation, and the > 700K alkene formation.

### **3.3. Reactions of Propan-2-ol on LaMnO<sub>3</sub>(100) versus La<sub>0.7</sub>Sr<sub>0.3</sub>MnO<sub>3</sub>(100)**

The adsorption and reaction of propan-2-ol has been used as a probe of acid-base properties on metal oxides.<sup>71-73</sup> As with ethanol, dehydration of propan-2-ol to produce propene occurs on acidic substrates. However, on reducible oxides, vacancies can abstract oxygen to form the alkene (with multiple elementary steps that can have the same stoichiometry as dehydration).

Dehydrogenation is known to occur on reducible oxides, and the hydrogen removed can either produce  $H_2$  or  $H_2O$ , with the carbon containing products ranging from the ketone to  $CO_x$  species. Of interest is whether the carbonyl formation can still occur with the same vacancy assisted mechanism given the branched alcohol. As with methanol and ethanol, we present the results of the PE-TPR experiments followed by those of the CE-TPR experiments.

### 3.3.1. PE-TPR of Propan-2-ol

Fig. 6 shows PE-TPR spectra following propan-2-ol adsorption at 190 K on oxidized  $LaMnO_3(100)$  and  $La_{0.7}Sr_{0.3}MnO_3(100)$ .

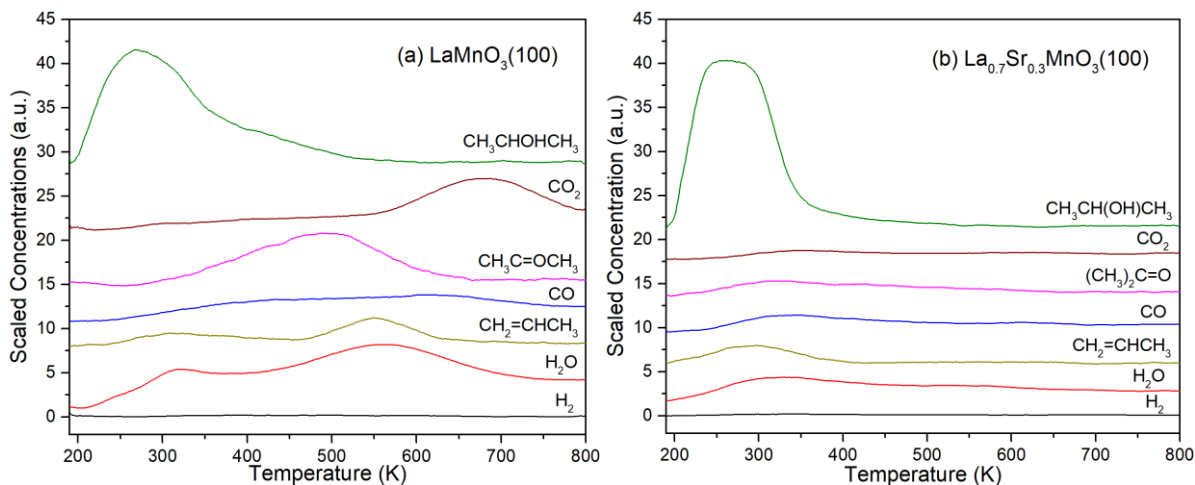
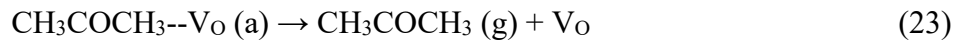
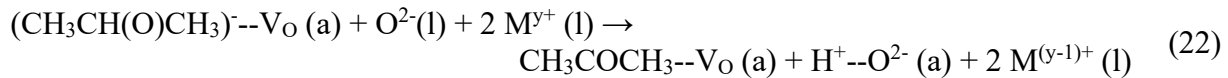
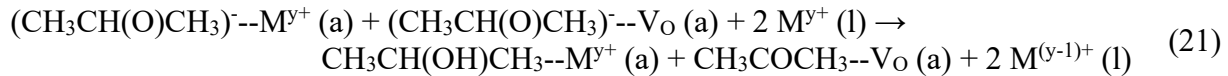
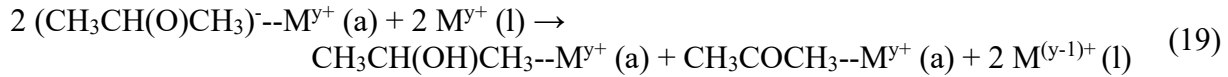
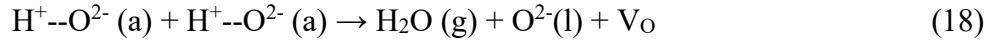


**Figure 6.** PE-TPR spectra following the adsorption of propan-2-ol at 190 K on pre-oxidized (a)  $LaMnO_3(100)$  and (b)  $La_{0.7}Sr_{0.3}MnO_3(100)$ .

The desorption of propan-2-ol and water from  $LaMnO_3(100)$  between 190 and 400 K are similar to what was observed for ethanol (Fig. 4a). Fig. 6a shows that propan-2-one is a major C-containing product between 400 and 600 K (analogous to the  $CH_3CHO$  peak in Fig. 4a). Both low temperature ( $\sim 300$  K) and high temperature ( $\sim 550$  K) water peaks are observed, as was observed for ethanol in Fig. 4a. As with ethanol, there are likely two different sources of the  $H_2O$ : now, from alkene production (propene in Fig. 6a) with stoichiometry equivalent to conventional

alcohol dehydration (more obvious in Fig. 6a than in Fig. 4a), but also still the water that originates from hydrogen extracted from alkoxies combining with surface O. As with ethanol, a portion of higher temperature H<sub>2</sub>O (~600 K) could be associated with a pathway for ketone formation via a pair of reactions with stoichiometry equivalent<sup>21, 69</sup> to disproportionation, without being a true disproportionation. For example, we cannot exclude the possibility that the ~500 K ketone comes from direct<sup>21, 34-35, 59, 61-64</sup> CH bond breaking from an alkoxy in an O-vacancy (Eq. 13). Similar to ethanol, we arrive at the following set of chemical reaction equations (with reaction 8 reproduced as Eq. 18 for clarity). Despite being a branched alcohol, the chemistry seems to be similar to that of ethanol. We assume that the alkoxy binds to V<sub>O</sub> and M<sup>y+</sup> sites via the oxygen, resulting in the reactions below. Eq. 2 is again reproduced as Eq. 18 for clarity and the notation is as described below Eq. 7.



As the surface continues to be heated, the surface intermediates decompose to form CO and CO<sub>2</sub>, similar to what was observed with ethanol. The amount of reaction products on La<sub>0.7</sub>Sr<sub>0.3</sub>MnO<sub>3</sub>(100) is much less than that on LaMnO<sub>3</sub>(100), which could be attributed to weaker interactions between propan-2-ol and the La<sub>0.7</sub>Sr<sub>0.3</sub>MnO<sub>3</sub>(100) surface. This speculation

is consistent with what we observed during methanol and ethanol adsorption in Section 3.1 and 3.2.

### 3.3.2. CE-TPR of Propan-2-ol with and without O<sub>2</sub>

The reactivity of propan-2-ol over LaMnO<sub>3</sub>(100) and La<sub>0.7</sub>Sr<sub>0.3</sub>MnO<sub>3</sub>(100) was further investigated with CE-TPR while the surface was exposed to alcohol with or without O<sub>2</sub>, as shown in Fig. 7. The alcohol flux was  $6.39 \times 10^{18}$  molecules m<sup>-2</sup> s<sup>-1</sup>, equal to a pressure of  $2.44 \times 10^{-6}$  Torr ( $3.25 \times 10^{-4}$  Pa) with respect to the sample surface.

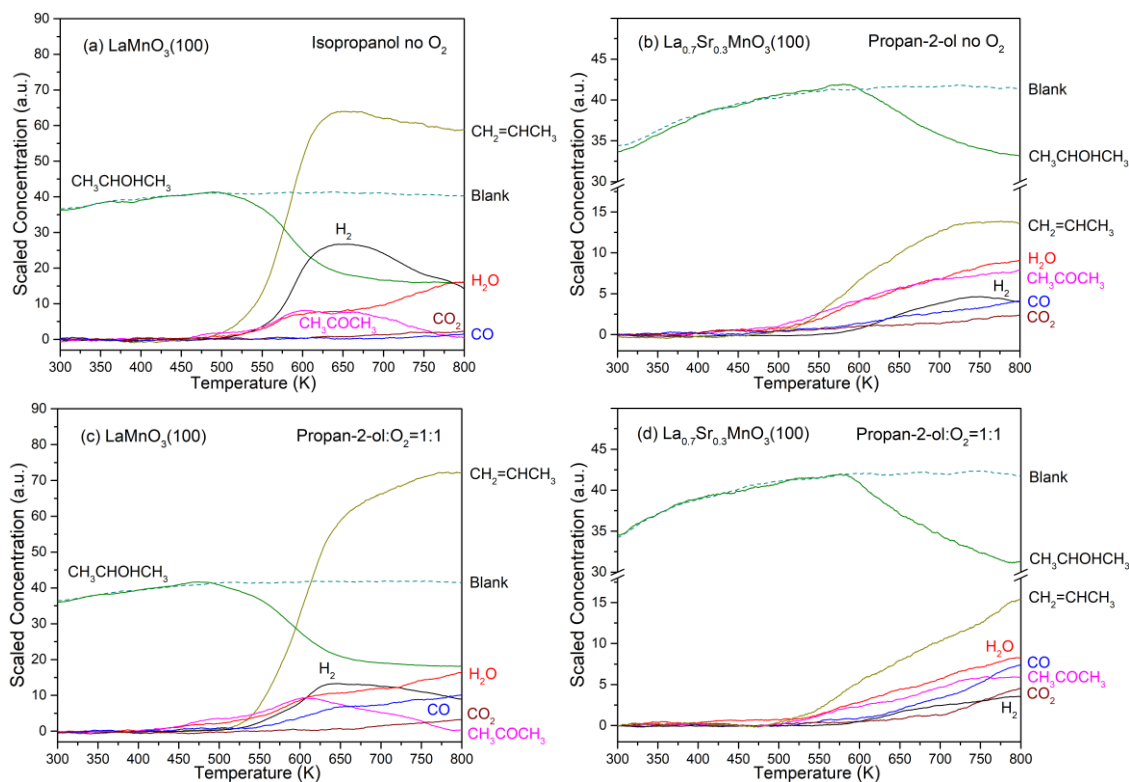


**Figure 7.** CE-TPR of propan-2-ol on LaMnO<sub>3</sub>(100) and La<sub>0.7</sub>Sr<sub>0.3</sub>MnO<sub>3</sub>(100) with the propan-2-ol:O<sub>2</sub> ratio set at 1:0 or 1:1. a) LaMnO<sub>3</sub>(100) and Ratio of 1:0, b) La<sub>0.7</sub>Sr<sub>0.3</sub>MnO<sub>3</sub>(100) and ratio of 1:0, c) LaMnO<sub>3</sub>(100) and Ratio of 1:1, d) La<sub>0.7</sub>Sr<sub>0.3</sub>MnO<sub>3</sub>(100) and ratio of 1:1.

In the absence of O<sub>2</sub>, dehydration and dehydrogenation of propan-2-ol begins at ~500 K to produce propan-2-one, propene, H<sub>2</sub> and water. As the surface is heated further, propan-2-one and molecular hydrogen production increases above 520 K. During heating LaMnO<sub>3</sub>(100) (above ~650 K), surface hydrogens can react with lattice oxygens and create oxygen vacancies. The presence of these oxygen vacancies could stabilize the propoxy intermediate on the surface enabling the greater activity observed at ~650 K.

On La<sub>0.7</sub>Sr<sub>0.3</sub>MnO<sub>3</sub>(100), propan-2-ol is much less reactive than on LaMnO<sub>3</sub>(100) but still more active than methanol or ethanol on La<sub>0.7</sub>Sr<sub>0.3</sub>MnO<sub>3</sub>(100), which is illustrated by the intensities of the reaction products. In the absence of O<sub>2</sub>, the major products are propene, propan-2-one, and water. At < 650 K, the formation rates of propene and propan-2-one are similar and the dehydration pathway is already competitive to the dehydrogenation mechanism, suggesting that the activation energy of breaking the β C-H bond and the C-O bond is comparable to that of breaking the α C-H bond.<sup>56</sup> Instead of combining with adsorbed hydrogen to produce molecular H<sub>2</sub> directly, H released from breaking the α C-H bond is generally assumed to be bound with the lattice O to form surface hydrogens, which can then go on to make H<sub>2</sub> or H<sub>2</sub>O. The reaction with lattice oxygen of surface hydrogens dominates H consumption below 570 K, as exhibited in Fig. 7b. The desorption of water creates oxygen vacancies that stabilize surface intermediates from propan-2-ol on La<sub>0.7</sub>Sr<sub>0.3</sub>MnO<sub>3</sub>(100). Above 650 K, there is more CO and CO<sub>2</sub> production than over LaMnO<sub>3</sub>(100).

When O<sub>2</sub> is present, propan-2-one production is more visible before 500K over LaMnO<sub>3</sub>(100), and is accompanied by the formation of water, presumably due to reaction of surface hydrogen with lattice oxygen. When the surface is further heated, propene and H<sub>2</sub> production become visible, along with increased propan-2-one and H<sub>2</sub>O production. Due to the

replenishment of lattice oxygens by O<sub>2</sub>, more lattice O is available and more CO<sub>x</sub> species are observed, along with more H<sub>2</sub>O, suggesting combustion-like pathways. The decrease in the rate of H<sub>2</sub> and propan-2-one production somewhat mirrors the increasing rate in water, CO<sub>x</sub> and propene formation: this may occur from a combination of surface hydrogens removing lattice oxygens, as well as simply due to the selectivity shift that occurs when more lattice oxygens are present (towards dehydration-type and combustion-like pathways). For CE-TPR on La<sub>0.7</sub>Sr<sub>0.3</sub>MnO<sub>3</sub>(100) in the presence of O<sub>2</sub>, the results are similar: increased alkene and CO<sub>x</sub> production, at the expense of propan-2-one.

### **3.4. Summary of Trends Observed Across the Experiments and Interpretation**

The trends observed across the experiments are largely consistent with published results from other reducible metal oxides, and a general summary of the common mechanistic pathways is provided here. At < 300K during PE-TPR, there is desorption of alcohols from molecular or recombination of alkoxy and hydrogen. Low temperature water production from hydroxy and lattice oxygen (250 K - 350K). One of the reviewers pointed out that if this alcohol is producing via a recombination reaction, the peaks for gas phase alcohol should shift to higher temperatures with lower initial coverages, in accordance with expectations for a TPR with a second order reaction between surface species.<sup>58</sup> While we did not systematically study the effects of coverage dependence, we did obtain some data to ensure that the pre-exposures being used were adequate. Those data are shown in the supporting information and do show the expected trend of the peak maximum shifting to higher temperature with lower coverages. Low temperature C-H bond breaking, presumably by disproportionation of pairs of adsorbates on non-vacancy sites, to produce alcohol and aldehydes/ketones (250-350K). For alcohols longer than C1, the intermediates of this mechanism may also go on to produce some alkenes in this temperature

range. Higher temperature C-H bond breaking occurs, presumably by disproportionation reactions with at least one of the adsorbates in an O-vacancy site (yielding 400-600K alcohol + aldehyde/ketone). This 400-600 K pathway is prominent for  $\text{LaMnO}_3(100)$ , and relatively suppressed for  $\text{La}_{0.7}\text{Sr}_{0.3}\text{MnO}_3(100)$ . The intermediates of this mechanism (surface alkoxies in vacancies) may also go on to produce some alkenes in this temperature range.<sup>36</sup> At  $\geq \sim 500$  K temperature range there may also be a contribution from direct CH bond breaking from an alkoxy in an O-vacancy (Eq. 6).

On  $\text{La}_{0.7}\text{Sr}_{0.3}\text{MnO}_3(100)$ , the alcohol desorption peaks increase in broadness with alcohol chain length: methanol < ethanol < propan-2-ol. Therefore, the residence times of the alcohols increase in this order, likely partially due to more dispersive interactions with longer chain lengths<sup>74-78</sup>. The stronger binding of the C3 intermediates relative to the C2 intermediates results in more  $\text{CO}_x$  from propan-2-ol relative to from ethanol. However, methanol produces the most  $\text{CO}_x$  species of the three alcohols: it may be that the dehydration pathway provides an outlet for strongly bound intermediates that prevents the more complete oxidation/composition. The lack of C-C bond breaking to produce  $\text{CO}_x$  species from methanol may also play a role in the greater quantity of  $\text{CO}_x$  species observed with methanol.

In the previous sections, PE-TPR results have shown that the alcohols are the primary products on both  $\text{LaMnO}_3(100)$  and  $\text{La}_{0.7}\text{Sr}_{0.3}\text{MnO}_3(100)$ , though this does not necessarily imply a lack of chemical reaction. The observed water formation is interpreted as being partially due to reaction of surface hydrogens with lattice oxygen, which creates oxygen vacancies and reduces the surface. During the course of the experiment, as water is produced with stoichiometric production of O vacancy sites, adsorbates can shift into O-vacancy sites into more strongly bonded states. The observation in Fig. 4 and Fig. 6 that the peak production of alkenes occurs at

higher temperature than that of the aldehydes/ketones is consistent with this interpretation: adsorbates more strongly bonded by their oxygen (within O-vacancies) can then break the C-O bond to make alkenes. The differences in temperatures of the major products in PE-TPR suggest that breakage of  $\alpha$  C-H bonds is easier than that of C-O or  $\beta$  C-H bonds on both surfaces, similar to published studies on cerium oxide.<sup>21, 23, 34-35, 38, 59, 63</sup> The extent of products observed increased in the order of methanol < ethanol < propan-2-ol, probably due to a combination of longer alcohols having stronger adsorption strengths and also more electron donation from the carbon backbone.

The CE-TPR experiments show the same products as PE-TPR, but with sustained production at primarily higher temperature ranges. At the temperatures at which products are observed in CE-TPR, >500 K, it is likely that direct C-H bond breaking occurs, and also that lattice oxygens are incorporated into the CO<sub>x</sub> and H<sub>2</sub>O species by Mars-Van Krevelen type reactions.<sup>70</sup> Given that direct C-H bond breaking may play a role at > 500K in CE-TPR, the pathways that are dominant at the <500K during PE-TPR experiments may become less relevant under continuous production at >500K. Based on  $1.04 \times 10^{19}$  surface cations per m<sup>2</sup>,<sup>38</sup> the 650 and 750 K turnover frequencies for the CE-TPR experiments are provided in Table 1 (obtained from the product molecules produced per site per second, based on the fluxes). These quantitative values reflect the selectivity and the activity described above, and can thus be used for comparison in kinetic modeling<sup>79</sup> studies to gain mechanistic insights into operative pathways.

**Table 1.** TOFs for C-containing products over LaMnO<sub>3</sub>(100) at 650 K and 750 K with alcohol flux equal to 3.25 x 10<sup>-4</sup> Pa

Alcohol (Reactant)	Product	Without O <sub>2</sub>		With 1:1 O <sub>2</sub>	
		650 K TOF(s <sup>-1</sup> )	750 K TOF(s <sup>-1</sup> )	650 K TOF(s <sup>-1</sup> )	750 K TOF(s <sup>-1</sup> )
Methanol	CO	1.82 x 10 <sup>-1</sup>	9.87 x 10 <sup>-1</sup>	1.54 x 10 <sup>-1</sup>	9.50 x 10 <sup>-1</sup>
	CO <sub>2</sub>	3.66 x 10 <sup>-2</sup>	8.87 x 10 <sup>-2</sup>	6.21 x 10 <sup>-2</sup>	7.41 x 10 <sup>-2</sup>
	H <sub>2</sub> CO	8.76 x 10 <sup>-2</sup>	2.07 x 10 <sup>-1</sup>	2.10 x 10 <sup>-1</sup>	2.39 x 10 <sup>-1</sup>
Ethanol	CO	< 3.0 x 10 <sup>-2</sup>	3.28 x 10 <sup>-2</sup>	< 3.0 x 10 <sup>-2</sup>	1.00 x 10 <sup>-1</sup>
	CO <sub>2</sub>	3.80 x 10 <sup>-2</sup>	6.53 x 10 <sup>-2</sup>	< 1.0 x 10 <sup>-2</sup>	6.18 x 10 <sup>-2</sup>
	CH <sub>3</sub> CHO	3.72 x 10 <sup>-2</sup>	< 3.0 x 10 <sup>-2</sup>	< 1.0 x 10 <sup>-2</sup>	6.18 x 10 <sup>-2</sup>
	CH <sub>2</sub> CH <sub>2</sub>	6.84 x 10 <sup>-1</sup>	9.28 x 10 <sup>-1</sup>	4.64 x 10 <sup>-1</sup>	1.04 x 10 <sup>0</sup>
Propan-2-ol	CO	< 1.0 x 10 <sup>-2</sup>	< 3.0 x 10 <sup>-2</sup>	9.96 x 10 <sup>-2</sup>	1.30 x 10 <sup>-1</sup>
	CO <sub>2</sub>	< 3.0 x 10 <sup>-2</sup>	3.02 x 10 <sup>-2</sup>	< 3.0 x 10 <sup>-2</sup>	3.31 x 10 <sup>-2</sup>
	CH <sub>3</sub> COCH <sub>3</sub>	1.13 x 10 <sup>-1</sup>	4.11 x 10 <sup>-2</sup>	1.10 x 10 <sup>-1</sup>	4.18 x 10 <sup>-2</sup>
	CH <sub>2</sub> CHCH <sub>3</sub>	9.53 x 10 <sup>-1</sup>	9.14 x 10 <sup>-1</sup>	8.63 x 10 <sup>-1</sup>	1.04 x 10 <sup>0</sup>

**Table 2.** TOFs for C-containing products over La<sub>0.7</sub>Sr<sub>0.3</sub>MnO<sub>3</sub>(100) at 650 K and 750 K with alcohol flux equal to 3.25 x 10<sup>-4</sup> Pa

Alcohol (Reactant)	Product	Without O <sub>2</sub>		With 1:1 O <sub>2</sub>	
		650 K TOF(s <sup>-1</sup> )	750 K TOF(s <sup>-1</sup> )	650 K TOF(s <sup>-1</sup> )	750 K TOF(s <sup>-1</sup> )
Methanol	CO	< 3.0 x 10 <sup>-2</sup>	1.08 x 10 <sup>-1</sup>	< 3.0 x 10 <sup>-2</sup>	1.12 x 10 <sup>-1</sup>
	CO <sub>2</sub>	< 3.0 x 10 <sup>-2</sup>	< 3.0 x 10 <sup>-2</sup>	< 3.0 x 10 <sup>-2</sup>	< 3.0 x 10 <sup>-2</sup>
	H <sub>2</sub> CO	4.62 x 10 <sup>-2</sup>	9.50 x 10 <sup>-2</sup>	4.70 x 10 <sup>-2</sup>	1.07 x 10 <sup>-1</sup>
Ethanol	CO	< 1.0 x 10 <sup>-2</sup>	< 3.0 x 10 <sup>-2</sup>	< 1.0 x 10 <sup>-2</sup>	< 3.0 x 10 <sup>-2</sup>
	CO <sub>2</sub>	< 1.0 x 10 <sup>-2</sup>	< 3.0 x 10 <sup>-2</sup>	< 1.0 x 10 <sup>-2</sup>	< 3.0 x 10 <sup>-2</sup>
	CH <sub>3</sub> CHO	3.05 x 10 <sup>-2</sup>	4.44 x 10 <sup>-2</sup>	4.56 x 10 <sup>-2</sup>	5.49 x 10 <sup>-2</sup>
	CH <sub>2</sub> CH <sub>2</sub>	< 3.0 x 10 <sup>-2</sup>	1.02 x 10 <sup>-1</sup>	4.58 x 10 <sup>-2</sup>	2.05 x 10 <sup>-1</sup>
Propan-2-ol	CO	3.27 x 10 <sup>-2</sup>	4.79 x 10 <sup>-2</sup>	< 3.0 x 10 <sup>-2</sup>	7.92 x 10 <sup>-2</sup>
	CO <sub>2</sub>	< 3.0 x 10 <sup>-2</sup>	< 3.0 x 10 <sup>-2</sup>	< 3.0 x 10 <sup>-2</sup>	4.42 x 10 <sup>-2</sup>
	CH <sub>3</sub> COCH <sub>3</sub>	8.49 x 10 <sup>-2</sup>	1.08 x 10 <sup>-1</sup>	4.87 x 10 <sup>-2</sup>	8.81 x 10 <sup>-2</sup>
	CH <sub>2</sub> CHCH <sub>3</sub>	1.47 x 10 <sup>-1</sup>	2.03 x 10 <sup>-1</sup>	1.21 x 10 <sup>-1</sup>	1.89 x 10 <sup>-1</sup>

During CE-TPR,  $\text{CO}_x$  products were observed in significant sustained quantities. There is evidence that oxidation of organic species with  $\text{LaMnO}_3$  perovskites may be limited by the oxidation potential at the surface (rather than by C-H bond breaking, for example).<sup>72</sup> Yet, a directly competing factor, the presence of oxygen vacancies, may be necessary to bind surface species strongly enough at  $> 500$  K, and thus the existence of oxygen vacancies may be more important for absolute activity.

The effects of Sr substitution in this study are thus worth considering. Partial surface blocking by Sr surface phases could account for part of the decrease in activity decrease in activity but would not be expected to show the same chemistry due to the lack of reducibility of Sr, and we thus consider how Sr substitution may affect the chemistry. The Sr substitution in  $\text{LaMnO}_3$  is expected to make a more easily reducible surface and/or increase the number of oxygen vacancies.<sup>40, 66, 80-82</sup> Yet in these experiments, products that are likely produced through adsorbates in vacancies are decreased. Prior to considering plausible interpretations, we note that in these experiments, both for PE-TPR and CE-TPR, not only the selectivity but also the activity may be influenced by surface residence times. One plausible explanation for why the Sr surface shows less activity in CE-TPR and PE-TPR is that at  $<10^{-4}$  Torr gas flux equivalent (including the case of no gas flux), the  $\text{La}_{0.7}\text{Sr}_{0.3}\text{MnO}_3$  surface may be largely devoid of surface species, leading to less reduction. Whereas over  $\text{LaMnO}_3$ , the surface residence times may be long enough to allow greater observed reactivity. A second plausible explanation may be related to the stability of the vacancies themselves: the Sr substituted perovskite may have more easily formed vacancies, but if the vacancies are more stable, they may bind adsorbates less strongly (again leading to less reactivity). The same trend of decreased overall activity with Sr substitution was observed for acetic acid conversion to ketene and combustion like products.<sup>14</sup>

Acetic acid is likely to bind sufficiently strongly to the surface that the latter plausible explanation may be the most credible: Sr substitution may result in vacancies that are less strongly binding, and thus less likely to affect the electronic structure of adsorbate molecules. Such an interpretation is chemically reasonable and has the important (but expected) implication that strategies to increase O-vacancy production by substitution may not always result in greater O-vacancy mediated catalytic activity. There may be increased oxygen transport from Sr substitution,<sup>68, 83</sup> though we doubt this plays a major role in the results of the present study (note that if oxygen transport was limiting, then we would expect higher oxidation activity from Sr substitution, which is not consistent with our results, and thus it is not likely that oxygen transport is limiting for the present study). Further studies are merited to better understand why Sr substitution decreases the overall activity. The situation may be further complicated if reconstruction occurs: studies of perovskite reconstruction with various pretreatments show that the perovskite surfaces tend to be enriched by A cation upon reconstruction with the formation of oxygen vacancies.<sup>84-86</sup> The extent of the Mn enrichment at the surface may also play a role.<sup>43</sup>

The presence of oxygen increased the relative yield of alkenes which are dehydration products (oxygen also increased a dehydration type pathway in experiments with acetic acid<sup>14</sup>). Given that the oxygen in the H<sub>2</sub>O comes from the alcohol for dehydration pathways (either directly or indirectly), the role of surface oxygen is likely to be that of a hydrogen acceptor for O-H bond breaking and C-H bond breaking. The mechanism presented here, with surface oxygen involved in H-abstraction during the dehydration pathway (to form alkenes) and not only the dehydrogenation pathway (to aldehydes/ketones) is in line with studies over cerium oxide<sup>34, 63</sup>. While surface oxygens play a role, we presently believe that most of the chemistry observed transpires via intermediates in O-vacancies, and that the chemistry for adsorbates bonded in O-

vacancies determines the selectivity in the PE-TPR and CE-TPR experiments in this study. In a study including infrared characterization of surface intermediates during catalytic conversion of alcohols over yttrium oxide,<sup>87</sup> bridge-bonded alkoxy species yielded propene at  $\geq \sim 250$  C (while a terminal bonded species gave propan-2-one): this is similar to our interpretation that the alkene production occurs at  $\geq \sim 500$ K via O-vacancy adsorbed intermediates, as an O-vacancy adsorbed alkoxy intermediate would be coordinated to the multiple cations exposed by the lattice O-vacancy. The mechanistic interpretations from the present study may be extensible to other reversibly reducible oxides.

#### 4. Conclusions

The surface chemistry and catalytic activity of small alcohols was studied over LaMnO<sub>3</sub>(100) and La<sub>0.7</sub>Sr<sub>0.3</sub>MnO<sub>3</sub>(100) thin films. Based on XPS data, both samples are manganese enriched relative to La in the surface region. The Sr substituted sample has enrichment of Sr near the surface relative to Mn and La. The chemistry that transpires over both surfaces shows similarity to what has been observed over some reducible oxides in the literature.

During PE-TPR, at  $< 300$ K, H<sub>2</sub>O is produced from surface hydrogens reacting with lattice oxygens. This results in vacancies such that some ethoxy groups would shift to vacancies very early in the PE-TPR experiment. At  $< 400$ K, there are two principle pathways for carbon-containing intermediates to leave the surface: there is facile desorption of alcohol (likely from a combination of molecular desorption as well as recombination of alkoxies and surface hydrogens), and also an alkoxy disproportionation reaction to produce alcohol and aldehyde/ketone consumes alkoxies on 'regular' cation sites (e.g.,  $2 \text{CH}_3\text{O} \rightarrow \text{products}$ ). Pathways involving oxygen vacancies occur at higher temperatures during PE-TPR: a) At  $\sim 400$ - $600$  K, the data is consistent with a second disproportionation reaction pathway between alkoxies

to produce alcohol and aldehyde/ketone that likely occurs between a pair of alkoxies where one is in an oxygen vacancy and one is on a 'regular' cation site b) when the alcohol chain length is > C1, a portion of the intermediates in oxygen vacancies also go through a pathway with dehydration stoichiometry to produce alkenes and water. The vacancy related pathways from 400-600 K are significantly suppressed by the Sr substitution. The branched structure of propan-2-ol did not suppress the reactions observed with ethanol. In fact, the extent of products observed increased in the order of methanol < ethanol < propan-2-ol, probably due to a combination of longer alcohols having stronger adsorption strengths and also more electron donation from the carbon backbone.

During CE-TPR, the products generally associated with dehydrogenation (aldehyde/ketone, H<sub>2</sub>), dehydration (alkene, H<sub>2</sub>O) and further oxidation (CO<sub>x</sub>, H<sub>2</sub>O) are observed with continuous production at temperatures > 500 K. Coupling products are not observed. For ethanol and propan-2-ol, the presence of oxygen increases the production of the alkene, H<sub>2</sub>O, and CO<sub>x</sub> species with diminishment of the H<sub>2</sub> and aldehyde/ketone production. For methanol, the effect of oxygen is less dramatic, though there is a clear increase of CO<sub>x</sub>, and H<sub>2</sub>O with a clear decrease of H<sub>2</sub>. For each of the alcohols, Sr substitution suppresses the overall activity towards nearly all pathways. At the temperatures at which products are observed in CE-TPR, >500 K, it is likely that direct C-H bond breaking occurs, and also that lattice oxygens are incorporated into the CO<sub>x</sub> and H<sub>2</sub>O species by Mars-Van Krevelen type reactions. The increase of alkenes in the presence of oxygen suggests that surface lattice oxygens play a role in the alkene production pathway, presumably for O-H and C-H bond breaking.

While Sr substitution would be expected to increase the number of lattice vacancies present, the PE-TPR and CE-TPR experiments here suggest a decrease in the products from

vacancy mediated related chemistry. These data are interpreted to mean that Sr substitution causes vacancies to bind adsorbates less strongly, resulting in decreased catalytic activity for the vacancy mediated reactions in the study. However, while Sr substitution does decrease the catalytic activity for the vacancy mediated reactions in the study, it does increase the ratio of alkene production to aldehyde/ketone production, which is useful information for catalytic science.

## AUTHOR INFORMATION

### Corresponding Author

\* savaraa@ornl.gov

\* mullinsdr@ornl.gov

## ACKNOWLEDGMENT

The authors thank Thomas Zac Ward and Christopher M. Rouleau for aid in the thin film growth. We thank one of the reviewers for helpful comments on the oxidation state equations. This work was supported by the U.S. Department of Energy, Office of Science, Office of Basic Energy Sciences, Chemical Sciences, Geosciences, and Biosciences Division, Catalysis Science. A portion of this research, the thin film growth and characterization, was conducted at the Center for Nanophase Materials Sciences, which is a DOE Office of Science User Facility. A portion of this research, the XPS measurements, used Beamline 23-ID-2 of the National Synchrotron Light Source II, a U.S. Department of Energy (DOE) Office of Science User Facility operated for the DOE Office of Science by Brookhaven National Laboratory under Contract No. DE-SC0012704.

**Supporting Information Available:** Explanation of “Approximated Charges” in Oxidation State Equations, and Figures Displaying the Shift of PE-TPR Alcohol Peaks To Higher Temperatures With Lower Coverages. This material is available free of charge via the Internet at <http://pubs.acs.org>.

## REFERENCES

- (1) Voorhoeve, R. J. H.; Johnson, D. W.; Remeika, J. P.; Gallagher, P. K. Perovskite Oxides: Materials Science in Catalysis. *Science* **1977**, *195*, 827-833.
- (2) Zhu, H.; Zhang, P.; Dai, S. Recent Advances of Lanthanum-Based Perovskite Oxides for Catalysis. *ACS Catalysis* **2015**, *5*, 6370-6385.
- (3) Zhu, J.; Li, H.; Zhong, L.; Xiao, P.; Xu, X.; Yang, X.; Zhao, Z.; Li, J. Perovskite Oxides: Preparation, Characterizations, and Applications in Heterogeneous Catalysis. *ACS Catalysis* **2014**, *4*, 2917-2940.
- (4) Misono, M. A View on the Future of Mixed Oxide Catalysts: The Case of Heteropolyacids (Polyoxometalates) and Perovskites. *Catalysis Today* **2005**, *100*, 95-100.
- (5) Tanaka, H.; Misono, M. Advances in Designing Perovskite Catalysts. *Current Opinion in Solid State and Materials Science* **2001**, *5*, 381-387.
- (6) Ciambelli, P.; Cimino, S.; De Rossi, S.; Lisi, L.; Minelli, G.; Porta, P.; Russo, G. A<sub>a</sub>FeO<sub>3</sub> (a=La, Nd, Sm) and LaFe<sub>1-x</sub>Mg<sub>x</sub>O<sub>3</sub> Perovskites as Methane Combustion and CO Oxidation Catalysts: Structural, Redox and Catalytic Properties. *Applied Catalysis B: Environmental* **2001**, *29*, 239-250.
- (7) Royer, S.; Duprez, D.; Can, F.; Courtois, X.; Batiot-Dupeyrat, C.; Laassiri, S.; Alamdari, H. Perovskites as Substitutes of Noble Metals for Heterogeneous Catalysis: Dream or Reality. *Chemical Reviews* **2014**, *114*, 10292-10368.
- (8) Nitadori, T.; Misono, M. Catalytic Properties of La<sub>1-x</sub>A'<sub>x</sub>FeO<sub>3</sub> (A' = Sr, Ce) and La<sub>1-x</sub>Ce<sub>x</sub>CoO<sub>3</sub>. *Journal of Catalysis* **1985**, *93*, 459-466.
- (9) Taihei, N.; Tatsumi, I.; Makoto, M. Catalytic Properties of Perovskite-Type Mixed Oxides (A<sub>2</sub>B<sub>2</sub>O<sub>7</sub>) Consisting of Rare Earth and 3d Transition Metals. The Roles of the A- and B-Site Ions. *Bulletin of the Chemical Society of Japan* **1988**, *61*, 621-626.
- (10) Newnham, R. E., Structure-Property Relationships in Perovskite Electroceramics. In *Perovskite: A Structure of Great Interest to Geophysics and Materials Science*, American Geophysical Union: 2013; pp 91-98.
- (11) Zwinkels, M. F. M.; Järås, S. G.; Menon, P. G.; Griffin, T. A. Catalytic Materials for High-Temperature Combustion. *Catalysis Reviews* **1993**, *35*, 319-358.
- (12) García de la Cruz, R. M.; Falcón, H.; Peña, M. A.; Fierro, J. L. G. Role of Bulk and Surface Structures of La<sub>1-x</sub>Sr<sub>x</sub>NiO<sub>3</sub> Perovskite-Type Oxides in Methane Combustion. *Applied Catalysis B: Environmental* **2001**, *33*, 45-55.
- (13) Ciambelli, P.; Cimino, S.; De Rossi, S.; Faticanti, M.; Lisi, L.; Minelli, G.; Pettiti, I.; Porta, P.; Russo, G.; Turco, M. AmnO<sub>3</sub> (a=La, Nd, Sm) and Sm<sub>1-x</sub>Sr<sub>x</sub>MnO<sub>3</sub> Perovskites as Combustion Catalysts: Structural, Redox and Catalytic Properties. *Applied Catalysis B: Environmental* **2000**, *24*, 243-253.
- (14) Zhang, Y.; Mullins, D. R.; Savara, A. Effect of Sr Substitution in LaMnO<sub>3</sub>(100) on Catalytic Conversion of Acetic Acid to Ketene and Combustion-Like Products. *The Journal of Physical Chemistry C* **2019**, *123*, 4148-4157.
- (15) Foo, G. S.; Polo-Garzon, F.; Fung, V.; Jiang, D.-e.; Overbury, S. H.; Wu, Z. Acid-Base Reactivity of Perovskite Catalysts Probed Via Conversion of 2-Propanol over Titanates and Zirconates. *ACS Catalysis* **2017**, *7*, 4423-4434.
- (16) Zhang, Y.; Savara, A.; Mullins, D. R. Ambient-Pressure Xps Studies of Reactions of Alcohols on SrTiO<sub>3</sub>(100). *The Journal of Physical Chemistry C* **2017**, *121*, 23436-23445.

- (17) Tan, S.; Gray, M. B.; Kidder, M. K.; Cheng, Y.; Daemen, L. L.; Lee, D.; Lee, H. N.; Ma, Y.-Z.; Doughty, B.; Lutterman, D. A. Insight into the Selectivity of Isopropanol Conversion at Strontium Titanate (100) Surfaces: A Combination Kinetic and Spectroscopic Study. *ACS Catalysis* **2017**, 8118-8129.
- (18) Idriss, H.; Barteau, M. A., Active Sites on Oxides: From Single Crystals to Catalysts. In *Advances in Catalysis*, Academic Press: 2000; Vol. 45, pp 261-331.
- (19) Badlani, M.; Wachs, I. E. Methanol: A “Smart” Chemical Probe Molecule. *Catalysis Letters* **2001**, 75, 137-149.
- (20) Savara, A. Simulation and Fitting of Complex Reaction Network Tpr: The Key Is the Objective Function. *Surface Science* **2016**, 653, 169-180.
- (21) Sutton, J. E.; Danielson, T.; Beste, A.; Savara, A. Below-Room-Temperature C–H Bond Breaking on an Inexpensive Metal Oxide: Methanol to Formaldehyde on CeO<sub>2</sub>(111). *The Journal of Physical Chemistry Letters* **2017**, 8, 5810-5814.
- (22) Albrecht, P. M.; Mullins, D. R. Adsorption and Reaction of Methanol over CeO<sub>x</sub>(100) Thin Films. *Langmuir* **2013**, 29, 4559-4567.
- (23) Beste, A.; Mullins, D. R.; Overbury, S. H.; Harrison, R. J. Adsorption and Dissociation of Methanol on the Fully Oxidized and Partially Reduced (111) Cerium Oxide Surface: Dependence on the Configuration of the Cerium 4f Electrons. *Surface Science* **2008**, 602, 162-175.
- (24) Mullins, D. R.; Albrecht, P. M.; Calaza, F. Variations in Reactivity on Different Crystallographic Orientations of Cerium Oxide. *Topics in Catalysis* **2013**, 56, 1345-1362.
- (25) Mullins, D. R.; Senanayake, S. D.; Chen, T. L. Adsorption and Reaction of C1–C3 Alcohols over CeO<sub>x</sub>(111) Thin Films. *The Journal of Physical Chemistry C* **2010**, 114, 17112-17119.
- (26) Calaza, F. C.; Xu, Y.; Mullins, D. R.; Overbury, S. H. Oxygen Vacancy-Assisted Coupling and Enolization of Acetaldehyde on CeO<sub>2</sub>(111). *Journal of the American Chemical Society* **2012**, 134, 18034-18045.
- (27) Chen, T. L.; Mullins, D. R. Adsorption and Reaction of Acetaldehyde over CeO<sub>x</sub>(111) Thin Films. *The Journal of Physical Chemistry C* **2011**, 115, 3385-3392.
- (28) Zhao, C.; Watt, C.; Kent, P. R.; Overbury, S. H.; Mullins, D. R.; Calaza, F. C.; Savara, A.; Xu, Y. Coupling of Acetaldehyde to Crotonaldehyde on CeO<sub>2</sub>–X(111): Bifunctional Mechanism and Role of Oxygen Vacancies. *The Journal of Physical Chemistry C* **2019**, 123, 8273-8286.
- (29) Idriss, H.; Diagne, C.; Hindermann, J. P.; Kiennemann, A.; Barteau, M. A. Reactions of Acetaldehyde on CeO<sub>2</sub> and CeO<sub>2</sub>-Supported Catalysts. *Journal of Catalysis* **1995**, 155, 219-237.
- (30) Idriss, H.; Kim, K. S.; Barteau, M. A. Carbon–Carbon Bond Formation Via Aldolization of Acetaldehyde on Single Crystal and Polycrystalline TiO<sub>2</sub> Surfaces. *Journal of Catalysis* **1993**, 139, 119-133.
- (31) Yee, A.; Morrison, S. J.; Idriss, H. A Study of the Reactions of Ethanol on CeO<sub>2</sub> and Pd/CeO<sub>2</sub> by Steady State Reactions, Temperature Programmed Desorption, and in Situ FT-IR. *Journal of Catalysis* **1999**, 186, 279-295.
- (32) Idriss, H. Surface Reactions of Uranium Oxide Powder, Thin Films and Single Crystals. *Surface Science Reports* **2010**, 65, 67-109.
- (33) Wilson, J. N.; Idriss, H. Reactions of Glutaric Acid on the TiO<sub>2</sub>(001) Single Crystal. Effect of Surface Reduction on the Reaction Pathway. *Langmuir* **2005**, 21, 8263-8269.

- (34) Beste, A.; Overbury, S. H. Dehydrogenation of Methanol to Formaldehyde Catalyzed by Pristine and Defective Ceria Surfaces. *Physical Chemistry Chemical Physics* **2016**, *18*, 9990-9998.
- (35) Sutton, J. E.; Overbury, S. H.; Beste, A. Coadsorbed Species Explain the Mechanism of Methanol Temperature-Programmed Desorption on CeO<sub>2</sub>(111). *The Journal of Physical Chemistry C* **2016**, *120*, 7241-7247.
- (36) Vohs, J. M. Site Requirements for the Adsorption and Reaction of Oxygenates on Metal Oxide Surfaces. *Chemical Reviews* **2013**, *113*, 4136-4163.
- (37) Guo, H.; Sun, D.; Wang, W.; Gai, Z.; Kravchenko, I.; Shao, J.; Jiang, L.; Ward, T. Z.; Snijders, P. C.; Yin, L.; Shen, J.; Xu, X. Growth Diagram of La<sub>0.7</sub>Sr<sub>0.3</sub>MnO<sub>3</sub> Thin Films Using Pulsed Laser Deposition. *Journal of Applied Physics* **2013**, *113*, 234301.
- (38) Beste, A. Methanol Adsorption and Dissociation on LaMnO<sub>3</sub> and Sr Doped LaMnO<sub>3</sub> (001) Surfaces. *Surface Science* **2017**, *664*, 155-161.
- (39) Shi, C.; Sun, L.; Qin, H.; Wang, X.; Li, L.; Hu, J. Adsorption Properties of CO Molecule on the Orthorhombic Structure LaMnO<sub>3</sub> (010) Surface. *Computational Materials Science* **2015**, *98*, 83-87.
- (40) Piskunov, S.; Heifets, E.; Jacob, T.; Kotomin, E. A.; Ellis, D. E.; Spohr, E. Electronic Structure and Thermodynamic Stability of LaMnO<sub>3</sub> and La<sub>1-x</sub>Sr<sub>x</sub>MnO<sub>3</sub> (001) Surfaces: Ab Initio Calculations. *Physical Review B* **2008**, *78*.
- (41) Chen, Y.; Téllez, H.; Burriel, M.; Yang, F.; Tsvetkov, N.; Cai, Z.; McComb, D. W.; Kilner, J. A.; Yildiz, B. Segregated Chemistry and Structure on (001) and (100) Surfaces of (La<sub>1-x</sub>Sr<sub>x</sub>)<sub>2</sub>CoO<sub>4</sub> Override the Crystal Anisotropy in Oxygen Exchange Kinetics. *Chemistry of Materials* **2015**, *27*, 5436-5450.
- (42) Lee, W.; Han, J. W.; Chen, Y.; Cai, Z.; Yildiz, B. Cation Size Mismatch and Charge Interactions Drive Dopant Segregation at the Surfaces of Manganite Perovskites. *Journal of the American Chemical Society* **2013**, *135*, 7909-7925.
- (43) Crumlin, E. J.; Mutoro, E.; Liu, Z.; Grass, M. E.; Biegalski, M. D.; Lee, Y.-L.; Morgan, D.; Christen, H. M.; Bluhm, H.; Shao-Horn, Y. Surface Strontium Enrichment on Highly Active Perovskites for Oxygen Electrocatalysis in Solid Oxide Fuel Cells. *Energy & Environmental Science* **2012**, *5*, 6081-6088.
- (44) Kotomin, E. A.; Mastrikov, Y. A.; Heifets, E.; Maier, J. Adsorption of Atomic and Molecular Oxygen on the LaMnO<sub>3</sub>(001) Surface: Ab Initio Supercell Calculations and Thermodynamics. *Physical Chemistry Chemical Physics* **2008**, *10*, 4644-4649.
- (45) Choi, Y.; Mebane, D. S.; Lin, M. C.; Liu, M. Oxygen Reduction on LaMnO<sub>3</sub>-Based Cathode Materials in Solid Oxide Fuel Cells. *Chemistry of Materials* **2007**, *19*, 1690-1699.
- (46) Tselev, A.; Vasudevan, R. K.; Gianfrancesco, A. G.; Qiao, L.; Ganesh, P.; Meyer, T. L.; Lee, H. N.; Biegalski, M. D.; Baddorf, A. P.; Kalinin, S. V. Surface Control of Epitaxial Manganite Films Via Oxygen Pressure. *ACS Nano* **2015**, *9*, 4316-4327.
- (47) Pilia, G.; Gao, P. X.; Ramprasad, R. Establishing the LaMnO<sub>3</sub> Surface Phase Diagram in an Oxygen Environment: An Ab Initio Kinetic Monte Carlo Simulation Study. *The Journal of Physical Chemistry C* **2012**, *116*, 26349-26357.
- (48) Hagans, P. L.; DeKoven, B. M.; Womack, J. L. A Laser Drilled Aperture for Use in an Ultrahigh Vacuum Gas Doser. *Journal of Vacuum Science & Technology A: Vacuum, Surfaces, and Films* **1989**, *7*, 3375-3377.

- (49) Wang, L.-Q.; Ferris, K. F.; Azad, S.; Engelhard, M. H. Adsorption and Reaction of Methanol on Stoichiometric and Defective SrTiO<sub>3</sub>(100) Surfaces. *The Journal of Physical Chemistry B* **2005**, *109*, 4507-4513.
- (50) Pauls, S. W.; Campbell, C. T. Magic-Angle Thermal Desorption Mass Spectroscopy. *Surface Science* **1990**, *226*, 250-256.
- (51) Miller, S. D.; Pushkarev, V. V.; Gellman, A. J.; Kitchin, J. R. Simulating Temperature Programmed Desorption of Oxygen on Pt(111) Using Dft Derived Coverage Dependent Desorption Barriers. *Topics in Catalysis* **2014**, *57*, 106-117.
- (52) Vestal, M. L.; Juhasz, P.; Martin, S. A. Delayed Extraction Matrix-Assisted Laser Desorption Time-of-Flight Mass Spectrometry. *Rapid Communications in Mass Spectrometry* **1995**, *9*, 1044-1050.
- (53) Savara, A.; Ludwig, W.; Schauermaun, S. Kinetic Evidence for a Non-Langmuir-Hinshelwood Surface Reaction: H/D Exchange over Pd Nanoparticles and Pd(111). *ChemPhysChem* **2013**, *14*, 1686-1695.
- (54) Ko, E. I.; Benziger, J. B.; Madix, R. J. Reactions of Methanol on W(100) and W(100)-(5 × 1)C Surfaces. *Journal of Catalysis* **1980**, *62*, 264-274.
- (55) Tatibouët, J. M. Methanol Oxidation as a Catalytic Surface Probe. *Applied Catalysis A: General* **1997**, *148*, 213-252.
- (56) Kim, K. S.; Barteau, M. A.; Farneth, W. E. Adsorption and Decomposition of Aliphatic Alcohols on Titania. *Langmuir* **1988**, *4*, 533-543.
- (57) Liu, Z.; Sorrell, C. C.; Koshy, P.; Hart, J. N. Dft Study of Methanol Adsorption on Defect-Free CeO<sub>2</sub> Low-Index Surfaces. *ChemPhysChem* **2019**, *20*, 2074-2081.
- (58) Masel, R. I., *Principles of Adsorption and Reaction on Solid Surfaces*. Wiley: New York, 1996; p xiv, 804.
- (59) Beste, A.; Overbury, S. H. Hydrogen and Methoxy Coadsorption in the Computation of the Catalytic Conversion of Methanol on the Ceria (111) Surface. *Surface Science* **2016**, *648*, 242-249.
- (60) Farneth, W. E.; Staley, R. H.; Sleight, A. W. Stoichiometry and Structural Effects in Alcohol Chemisorption Temperature-Programmed Desorption on Molybdenum Trioxide. *Journal of the American Chemical Society* **1986**, *108*, 2327-2332.
- (61) Kropp, T.; Paier, J. Activity Versus Selectivity of the Methanol Oxidation at Ceria Surfaces: A Comparative First-Principles Study. *The Journal of Physical Chemistry C* **2015**, *119*, 23021-23031.
- (62) Kropp, T.; Paier, J. Reactions of Methanol with Pristine and Defective Ceria (111) Surfaces: A Comparison of Density Functionals. *The Journal of Physical Chemistry C* **2014**, *118*, 23690-23700.
- (63) Beste, A.; Overbury, S. H. Pathways for Ethanol Dehydrogenation and Dehydration Catalyzed by Ceria (111) and (100) Surfaces. *The Journal of Physical Chemistry C* **2015**, *119*, 2447-2455.
- (64) Capdevila-Cortada, M.; García-Melchor, M.; López, N. Unraveling the Structure Sensitivity in Methanol Conversion on CeO<sub>2</sub>: A Dft+U Study. *Journal of Catalysis* **2015**, *327*, 58-64.
- (65) Zhu, J.; Mu, W.; Su, L.; Li, X.; Guo, Y.; Zhang, S.; Li, Z. Al-Doped TiO<sub>2</sub> Mesoporous Material Supported Pd with Enhanced Catalytic Activity for Complete Oxidation of Ethanol. *Journal of Solid State Chemistry* **2017**, *248*, 142-149.

- (66) Wang, W.; Zhang, H.-b.; Lin, G.-d.; Xiong, Z.-t. Study of Ag/La<sub>0.6</sub>Sr<sub>0.4</sub>MnO<sub>3</sub> Catalysts for Complete Oxidation of Methanol and Ethanol at Low Concentrations. *Applied Catalysis B: Environmental* **2000**, *24*, 219-232.
- (67) Duan, Q.; Wang, J.; Ding, C.; Ding, H.; Guo, S.; Jia, Y.; Liu, P.; Zhang, K. Partial Oxidation of Methane over Ni Based Catalyst Derived from Order Mesoporous Lanthanum Perovskite Prepared by Modified Nanocasting Method. *Fuel* **2017**, *193*, 112-118.
- (68) Shimizu, T. Activity of Ethanol Oxidation to Acetaldehyde over La<sub>1-x</sub>Sr<sub>x</sub>FeO<sub>3</sub> and La<sub>1-x</sub>Mn<sub>x</sub>FeO<sub>3</sub> (Me=Co, Mn, Ni, Fe). *Applied Catalysis* **1986**, *28*, 81-88.
- (69) Savara, A.; Chan-Thaw, C. E.; Rossetti, I.; Villa, A.; Prati, L. Benzyl Alcohol Oxidation on Carbon-Supported Pd Nanoparticles: Elucidating the Reaction Mechanism. *ChemCatChem* **2014**, *6*, 3464-3473.
- (70) Mullins, D. R. The Surface Chemistry of Cerium Oxide. *Surface Science Reports* **2015**, *70*, 42-85.
- (71) Chen, H.; Zhang, H.; Yan, Y. Gradient Porous Co-Cu-Mn Mixed Oxides Modified ZSM-5 Membranes as High Efficiency Catalyst for the Catalytic Oxidation of Isopropanol. *Chemical Engineering Science* **2014**, *111*, 313-323.
- (72) Spinicci, R.; Faticanti, M.; Marini, P.; De Rossi, S.; Porta, P. Catalytic Activity of LaMnO<sub>3</sub> and LaCoO<sub>3</sub> Perovskites Towards VOCs Combustion. *Journal of Molecular Catalysis A: Chemical* **2003**, *197*, 147-155.
- (73) Kulkarni, D.; Wachs, I. E. Isopropanol Oxidation by Pure Metal Oxide Catalysts: Number of Active Surface Sites and Turnover Frequencies. *Applied Catalysis A: General* **2002**, *237*, 121-137.
- (74) Tait, S. L.; Dohnálek, Z.; Campbell, C. T.; Kay, B. D. N-Alkanes on Pt(111) and on C(0001) / Pt(111): Chain Length Dependence of Kinetic Desorption Parameters. *The Journal of Chemical Physics* **2006**, *125*, 234308.
- (75) Dostert, K. H.; O'Brien, C. P.; Liu, W.; Riedel, W.; Savara, A.; Tkatchenko, A.; Schauermaun, S.; Freund, H. J. Adsorption of Isophorone and Trimethyl-Cyclohexanone on Pd(111): A Combination of Infrared Reflection Absorption Spectroscopy and Density Functional Theory Studies. *Surface Science* **2016**, *650*, 149-160.
- (76) Dostert, K. H.; O'Brien, C. P.; Riedel, W.; Savara, A.; Liu, W.; Oehzelt, M.; Tkatchenko, A.; Schauermaun, S. Interaction of Isophorone with Pd(111): A Combination of Infrared Reflection-Absorption Spectroscopy, near-Edge X-Ray Absorption Fine Structure, and Density Functional Theory Studies. *J Phys Chem C* **2014**, *118*, 27833-27842.
- (77) Liu, W.; Jiang, Y. D.; Dostert, K. H.; O'Brien, C. P.; Riedel, W.; Savara, A.; Schauermaun, S.; Tkatchenko, A. Catalysis Beyond Frontier Molecular Orbitals: Selectivity in Partial Hydrogenation of Multi-Unsaturated Hydrocarbons on Metal Catalysts. *Sci Adv* **2017**, *3*.
- (78) Liu, W.; Savara, A.; Ren, X. G.; Ludwig, W.; Dostert, K. H.; Schauermaun, S.; Tkatchenko, A.; Freund, H. J.; Scheffler, M. Toward Low-Temperature Dehydrogenation Catalysis: Isophorone Adsorbed on Pd(111). *J Phys Chem Lett* **2012**, *3*, 582-586.
- (79) Matera, S.; Schneider, W. F.; Heyden, A.; Savara, A. Progress in Accurate Chemical Kinetic Modeling, Simulations, and Parameter Estimation for Heterogeneous Catalysis. *ACS Catalysis* **2019**, *9*, 6624-6647.
- (80) Kuo, J. H.; Anderson, H. U.; Sparlin, D. M. Oxidation-Reduction Behavior of Undoped and Sr-Doped LaMnO<sub>3</sub> Nonstoichiometry and Defect Structure. *Journal of Solid State Chemistry* **1989**, *83*, 52-60.

- (81) Fernandez-Torre, D.; Carrasco, J.; Ganduglia-Pirovano, M. V.; Perez, R. Hydrogen Activation, Diffusion, and Clustering on CeO<sub>2</sub>(111): A Dft+U Study. *J Chem Phys* **2014**, *141*.
- (82) Peng, Y.; Si, W.; Li, J.; Crittenden, J.; Hao, J. Experimental and Dft Studies on Sr-Doped LaMnO<sub>3</sub> Catalysts for Nox Storage and Reduction. *Catalysis Science & Technology* **2015**, *5*, 2478-2485.
- (83) Lee, D.; Lee, Y. L.; Wang, X. R.; Morgan, D.; Shao-Horn, Y. Enhancement of Oxygen Surface Exchange on Epitaxial La<sub>0.6</sub>Sr<sub>0.4</sub>Co<sub>0.2</sub>Fe<sub>0.8</sub>O<sub>3-Δ</sub> Thin Films Using Advanced Heterostructured Oxide Interface Engineering. *Mrs Commun* **2016**, *6*, 204-209.
- (84) Polo-Garzon, F.; Yang, S.-Z.; Fung, V.; Foo, G. S.; Bickel, E. E.; Chisholm, M. F.; Jiang, D.-e.; Wu, Z. Controlling Reaction Selectivity through the Surface Termination of Perovskite Catalysts. *Angewandte Chemie* **2017**, *129*, 9952-9956.
- (85) Dagdeviren, O. E.; Simon, G. H.; Zou, K.; Walker, F. J.; Ahn, C.; Altman, E. I.; Schwarz, U. D. Surface Phase, Morphology, and Charge Distribution Transitions on Vacuum and Ambient Annealed SrTiO<sub>3</sub>. *Physical Review B* **2016**, *93*, 195303.
- (86) Ngai, J. H.; Schwendemann, T. C.; Walker, A. E.; Segal, Y.; Walker, F. J.; Altman, E. I.; Ahn, C. H. Achieving a-Site Termination on La<sub>0.18</sub>Sr<sub>0.82</sub>Al<sub>0.59</sub>Ta<sub>0.41</sub>O<sub>3</sub> Substrates. *Advanced Materials* **2010**, *22*, 2945-2948.
- (87) Hussein, G. A. M.; Gates, B. C. Surface and Catalytic Properties of Yttrium Oxide: Evidence from Infrared Spectroscopy. *Journal of Catalysis* **1998**, *176*, 395-404.

TOC Figure:

